




Complex Reactive Acids from Methanol and Carbon Dioxide Ice: Glycolic Acid (HOCH₂COOH) and Carbonic Acid Monomethyl Ester (CH₃OCOOH)

Joshua H. Marks^{1,2} , Jia Wang^{1,2} , Mikhail M. Evseev³ , Oleg V. Kuznetsov³ , Ivan O. Antonov³, and Ralf I. Kaiser^{1,2} 

¹W. M. Keck Research Laboratory in Astrochemistry, University of Hawaii at Manoa, Honolulu, HI 96822, USA; ralfk@hawaii.edu

²Department of Chemistry, University of Hawaii at Manoa, Honolulu, HI 96822, USA

³Center for Laboratory Astrophysics, Lebedev Physical Institute of the Russian Academy of Sciences (LPIRAS), Samara, 443011, Russia; pfizeke@gmail.com

Received 2022 August 2; revised 2022 September 21; accepted 2022 October 4; published 2023 January 6

Abstract

The formation of complex organic molecules by simulated secondary electrons generated in the track of galactic cosmic rays was investigated in interstellar ice analogs composed of methanol and carbon dioxide. The processed ices were subjected to temperature-programmed desorption to mimic the transition of a cold molecular cloud to a warmer star-forming region. Reaction products were detected as they sublime using photoionization reflectron time-of-flight mass spectrometry. By employing isotopic labeling, tunable photoionization and computed adiabatic ionization energies isomers of C₂H₄O₃ were investigated. Product molecules carbonic acid monomethyl ester (CH₃OCOOH) and glycolic acid (HOCH₂COOH) were identified. The abundance of the reactants detected in analog interstellar ices and the low irradiation dose necessary to form these products indicates that these molecules are exemplary candidates for interstellar detection. Molecules sharing a tautomeric relationship with glycolic acid, dihydroxyacetaldehyde ((OH)₂CCHO), and the enol ethenetriol (HOCHC(OH)₂), were not found to form despite ices being subjected to conditions that have successfully produced tautomerization in other ice analog systems.

Unified Astronomy Thesaurus concepts: Laboratory astrophysics (2004); Interstellar molecules (849); Radical-radical recombination (1071); Pre-biotic astrochemistry (2079); Astrochemistry (75)

1. Introduction

Complex organic molecules (COMs)—by astronomical definition are organic molecules with six or more atoms—comprising hydrogen, carbon, and oxygen observed in the interstellar medium (ISM) carry functional groups such as alcohols (ROH), ethers (ROR'), aldehydes (RCHO), ketones (RCOR'), and esters (RCOOR') (Herbst & van Dishoeck 2009; Turner & Kaiser 2020). One of the primary motivations behind laboratory astrochemistry is to develop a fundamental understanding of how key classes of COMs form abiotically and fit into reaction pathways to synthesize molecules of astrobiological importance such as amino acids (Muñoz Caro et al. 2002; Holtom et al. 2005; de Marcellus et al. 2011; Kaiser et al. 2013; Nuevo et al. 2007, 2008), dipeptides (Kaiser et al. 2013), alcohols (Bernstein Max et al. 1999; Bennett et al. 2005b; Kaiser et al. 2015; Bergantini et al. 2017; Fedoseev et al. 2017; Bergantini et al. 2018; Zhu et al. 2019; Kleimeier & Kaiser 2021), and glycerol phosphates (Zhu et al. 2020a). These molecules are the building blocks of all living organisms, e.g., proteins, nucleotides, and cell membranes (Plankensteiner et al. 2005; Kitadai & Maruyama 2018). A greater understanding of the formation mechanisms of distinct structural isomers—molecules that share a molecular formula but differ in connectivity—is vital because isomer-specific information can be used in astrochemical modeling to trace the chemical and physical conditions in the ISM (Abplanalp et al. 2016b). At present, the formation mechanisms of the majority of COMs are partially understood and astrochemical models based on *gas-phase-only chemistry* substantially underpredict the interstellar abundance of COMs such as methyl formate

(HCOOCH₃), dimethyl ether ((CH₃)₂O), and acetaldehyde (CH₃CHO) (Petrie 1995; Kaiser 2002; Garrod et al. 2006, 2008; Herbst 2021). Predominantly, astrochemical models approximate interstellar ices as largely inert and consider only surface reactions despite strong evidence that galactic cosmic rays (GCRs) can penetrate ice mantles and initiate the formation of COMs (Turner & Kaiser 2020).

Oxygen plays a pivotal role in biochemistry as this electronegative element can produce local dipoles upon bond formation with, e.g., hydrogen and carbon, which allow for a wide range of chemical reactions unavailable to hydrocarbons. Highly oxygenated molecules such as carbonic acid monomethyl ester (CH₃OCOOH, (1), glycolic acid (HOCH₂COOH, (2), ethenetriol (HOCHC(OH)₂, (3), and dihydroxyacetaldehyde ((OH)₂CCHO, (4) (Figure 1) have yet to be detected in the ISM; in addition, no detections of molecules containing three or more oxygen atoms have been reported in the gas phase. Nevertheless, several molecules bearing structural similarities to the species shown as products in Figure 1 are known in the ISM; while no carbonic esters (ROCOOR') or hemiesters (ROCOOH) have been detected in the ISM yet, several related molecules containing esters have been identified. For instance, methyl formate (CH₃COOH) was first tentatively observed in the *cis* configuration by Brown et al. (1975) toward Sgr B2 using the Parkes 64 m telescope on the basis of two lines near 1.6 GHz. In more recent observations using the Green Bank telescope Neill et al. (2012) identified the presence of *trans*-methyl formate toward Sgr B2(N), and van Scheltinga et al. (2021) tentatively identified the presence of methyl formate in the Spitzer survey toward the nebula HH 46. Substitution of the carboxylic acid moiety in glycolic acid (2) for an aldehyde yields glycolaldehyde (HOCH₂CHO), which was first detected in the molecular cloud Sgr B2(N) by Hollis et al. (2000) with the NRAO 12 m telescope using four unblended and two blended lines in the 71–104 GHz range.



Original content from this work may be used under the terms of the [Creative Commons Attribution 4.0 licence](https://creativecommons.org/licenses/by/4.0/). Any further distribution of this work must maintain attribution to the author(s) and the title of the work, journal citation and DOI.

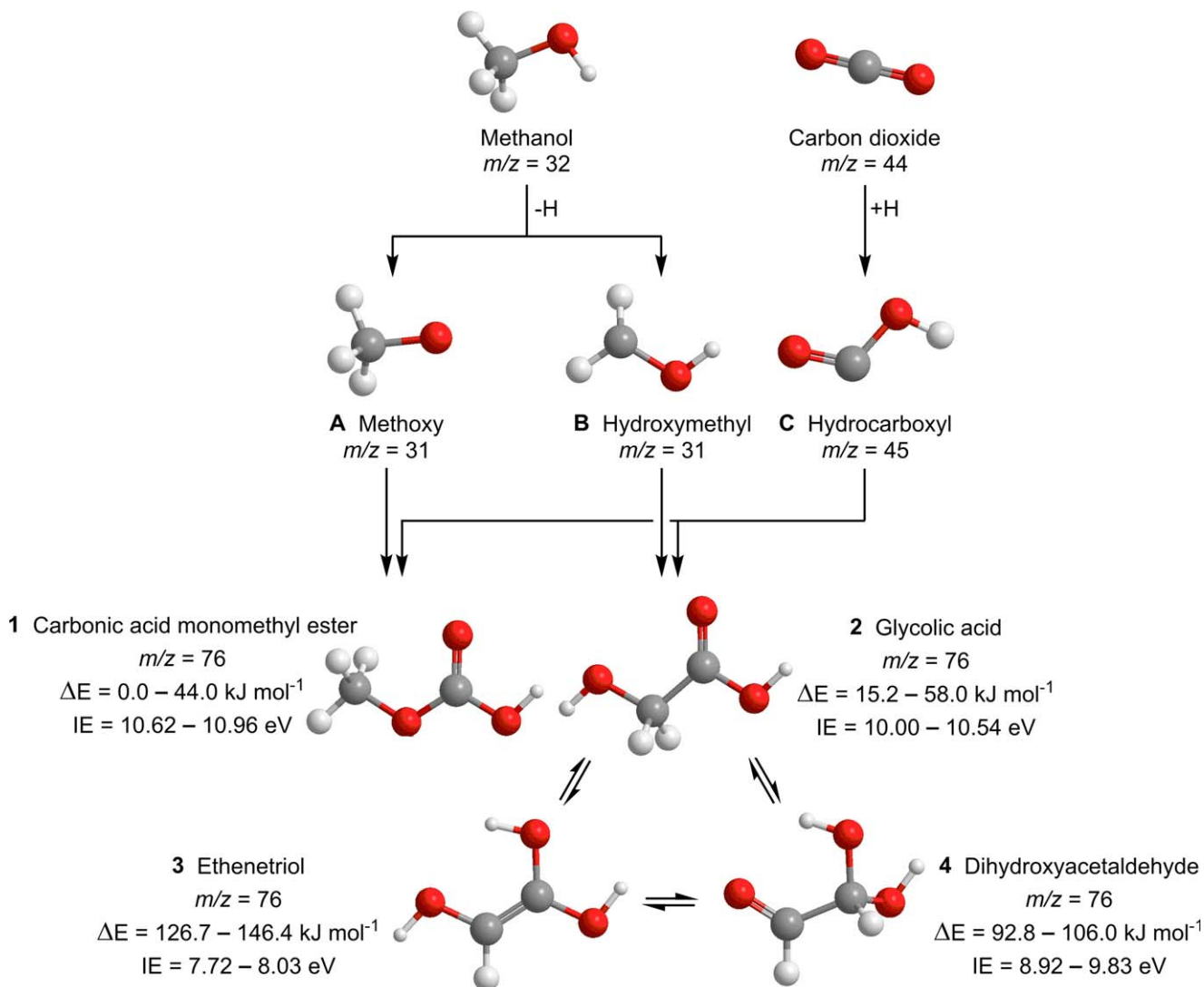


Figure 1. Reaction scheme leading to four isomers of $C_2H_4O_3$. Computed relative energies and adiabatic ionization energies (IEs) are presented as ranges that include all conformers.

More recent work by Jørgensen et al. (2012) also identified glycolaldehyde toward IRAS 16293-2422. The detection of the enol isomer of glycolaldehyde ($HOCH_2CHO$), which forms via a hydrogen shift to produce an $R^1R^2C=C(OH)R^3$ substructure, was reported in laboratory astrochemistry experiments by Kleimeier & Kaiser (2022) and in deep space by Rivilla et al. (2022). *Z*-1,2-ethenediol ($HOCHCHOH$), only one hydroxyl group ($-OH$) away from ethenetriol (3), was detected toward the molecular cloud G+0.693-0.027 with the 40 m Yebes and the 30 m IRAM telescopes on the basis of 18 unblended or slightly blended transitions in the range of 35–95 GHz, also reported by Rivilla et al. (2022). The COMs listed above are all similar in that they contain two oxygen atoms and have been detected toward molecular clouds.

Carbonic acid monomethyl ester (1) exemplifies a hemiester of carbonic acid, where a hemiester is the result of esterification of only one carboxylic acid group in a molecule that contains more than one. Being only partially esterified, this molecule is highly susceptible to subsequent addition by nucleophiles, e.g., alcohols (ROH) or amines (e.g., RNH_2) (Dibenedetto et al. 2006). As the simplest α -hydroxy carboxylic acid, glycolic acid (2) is an example of a class of bifunctional molecules in

which a hydroxyl moiety (ROH) is adjacent to a carboxylic acid (RCOOH). It is related glycolaldehyde ($HOCH_2CHO$) by substitution of the hydrogen in the aldehyde group ($-CHO$) with a hydroxyl ($-OH$) to form an acid ($-COOH$). Glycolic acid (2), glycolaldehyde ($HOCH_2CHO$), and ethylene glycol ($HOCH_2CH_2OH$) have all been observed in the soluble organic fraction of carbonaceous chondrites such as the Murchison meteorite (Peltzer & Bada 1978; Peltzer et al. 1984). These are the smallest sugar-related molecules and investigation of their routes of formation may aid in understanding the origin of prebiotic molecules necessary for the origins of life (Braakman et al. 2010; Bossa et al. 2014; Meinert et al. 2016; Zhou et al. 2020).

Investigations focusing on the vibrational and electronic structures of carbonic acid monomethyl ester (1) have relied on the protonation of methyl carbonate salt ($NaOCOOCH_3$) (Dibenedetto et al. 2006), decomposition of a larger carbonic diester *tert*-butyl methyl carbonate ($((CH_3)_3COC(O)OCH_3$) (Reisenauer et al. 2014; Linden et al. 2018), or its aqueous formation in trace quantities by condensation of bicarbonate salt ($NaHCO_3$) and methanol (CH_3OH) (Köck et al. 2020). To date, carbonic acid monomethyl ester (1) has not been studied

experimentally with respect to its potential formation in environments relevant to astrochemistry. Numerous synthetic methods have been suggested for the production of glycolic acid (2) in environments relevant to astrochemistry. Bottom-up syntheses based on the irradiation of interstellar ice analogs composed of mixtures of carbon monoxide (CO), carbon dioxide (CO₂), water (H₂O), methanol (CH₃OH), and ammonia (NH₃), or some subset thereof, have repeatedly produced glycolic acid (Agarwal et al. 1985; Briggs et al. 1992; Nuevo et al. 2010; Meinert et al. 2016; Paardekooper et al. 2016). The stability and low vapor pressure of glycolic acid allow for identification through offline gas-chromatography mass spectrometry with which the complex mixture of reaction products were analyzed. However, the complexity of these mixtures precludes an assessment of the mechanism by which glycolic acid (2) forms. Top-down synthesis of glycolic acid (2) and other products from pyruvate during meteor impact has been proposed by Cooper et al. (2011) as an explanation for the abundance of sugar-related molecules in the Murchison meteorite. Reactions based on the Strecker synthesis have also been proposed as a route to the formation of glycolic acid (2) in addition to several other α -hydroxy carboxylic acids (-CH(OH)COOH), many of which are abundant in carbonaceous chondrites (Peltzer & Bada 1978; Peltzer et al. 1984). Irradiation of pure methanol ice with low-energy electrons has also been observed to form glycolic acid (2), because this experiment was designed to identify possible reaction products rather than mechanistic information, the formation mechanism remains unknown (Boamah et al. 2014).

As shown above, glycolic acid (2) can be formed by numerous routes, but sophisticated experiments are needed to untangle reaction mechanisms relevant to the chemistry of icy grains. Decomposition of methanol (CH₃OH) upon exposure to galactic cosmic rays (GCRs), or their energetic secondary electrons, has been shown to yield radical intermediates methoxy (CH₃O $\dot{\text{C}}$) and hydroxymethyl ($\dot{\text{C}}\text{H}_2\text{OH}$) (Bennett et al. 2007; Maity et al. 2014; Kaiser et al. 2015; Góbi et al. 2018; Bergantini et al. 2018; Zhu et al. 2020a, 2020b; Kleimeier et al. 2021; Zhu et al. 2022). These processes are endoergic by 218.8 ± 0.3 and 200.5 ± 0.3 kJ mol⁻¹ (Ruscic & Bross 2021), respectively, and can be accessed through kinetic energy contributed by GCRs impinging on the molecules of the ices (Kaiser et al. 1997). Methanol ice is abundant in the ISM, with concentrations in ices of up to 30% relative to water toward star-forming regions (White et al. 2003; Fuente et al. 2014) and low-mass protostar IRAS 16293-2422 (Parise et al. 2002; Cazaux et al. 2003). Ices containing carbon dioxide (CO₂) and a source of atomic hydrogen can produce hydroxycarbonyl radical (HO $\dot{\text{C}}\text{O}$), which is capable of adding a carboxylic acid moiety to another radical via recombination (Turner et al. 2021; Kleimeier & Kaiser 2022). The barrier of hydrogen atom addition to carbon dioxide to form hydroxycarbonyl has been calculated to be 111 kJ mol⁻¹ for the *cis* isomer and 144 kJ mol⁻¹ for the *trans* isomer (Song et al. 2006), and can be overcome by suprathreshold hydrogen atoms formed within the ices through GCR interaction with the molecular components (Morton & Kaiser 2003). Carbon dioxide (CO₂) has been found in abundance in interstellar ices toward a number of molecular clouds and young solar objects, and concentrations relative to water in excess of 50% have been reported (Gibb et al. 2004).

Here, we present laboratory experiments on the formation of carbonic acid monomethyl ester (CH₃OCOOH, 1) and glycolic acid (HOCH₂COOH, 2) in low-temperature model interstellar ices composed of methanol (CH₃OH) and carbon dioxide (CO₂) based on the reaction scheme shown in Figure 1. The binary mixed ices were irradiated at a temperature of 5 K with energetic electrons, which simulate secondary electrons produced by the passage of GCRs to initiate nonequilibrium chemistry vital to the formation of COMs (Bennett et al. 2005a). Ices were exposed to irradiation doses of 0.45–11 eV per molecule of methanol and 0.60–14 eV per molecule of carbon dioxide, equivalent to a few 10⁶ to 10⁷ yr of exposure to GCRs in the interior of a molecular cloud (Yeghikyan 2011). These experiments employ broadly tunable single photon photoionization (PI) and reflectron time-of-flight mass spectrometry (ReToF-MS) as a highly sensitive, *isomer-selective* technique (Abplanalp et al. 2016a; Turner & Kaiser 2020; Zhu et al. 2021). Products subliming during temperature-programmed desorption (TPD) from 5–320 K were photoionized and mass analyzed. Isotopic labeling of the reactants permits unambiguous assignment of the observed ions to the formula C₂H₄O₃. These methods allow for detailed insights into the mechanism of the formation of observed isomers (Turner & Kaiser 2020). Our experiments show clear evidence for the formation of carbonic acid monomethyl ester (1) and glycolic acid (2) in these methanol–carbon dioxide ices. Despite employing irradiation doses that have been shown previously to produce tautomerization in other systems (Abplanalp et al. 2016b; Kleimeier et al. 2020, 2021; Kleimeier & Kaiser 2021, 2022), these isomerization reactions do not produce the tautomers ethenetriol (3) and dihydroxyacetaldehyde (4). These results are significant findings in the understanding of the formation pathways of key COMs available to interstellar ice chemistry deep inside interstellar ices through GCR-induced nonequilibrium chemistries.

2. Methods

2.1. Experimental Methods

The experiments reported here were carried out at the W. M. Keck Research Laboratory in Astrochemistry (Jones & Kaiser 2013; Abplanalp et al. 2016a, 2016b). The apparatus consists of a hydrocarbon-free stainless steel ultrahigh vacuum chamber with pressures maintained at a few 10⁻¹¹ Torr by magnetically levitated turbomolecular pumps (Kaiser et al. 2014). A closed cycle Gifford-McMahon helium cryostat (Sumitomo Heavy Industries, RDK-415E) is used to maintain a mirror-polished silver wafer (12.6 × 15.1 mm) at 5.0 ± 0.2 K. The cryostat/wafer assembly is rotatable within the horizontal plane using a doubly differentially pumped rotatable flange (Thermionics Vacuum Products, RNN-600/FA/MCO), and vertically translatable via an adjustable bellows (McAllister, BLT106). Ices studied were prepared by passing methanol vapor (Fisher Scientific, >99.8%) and gaseous carbon dioxide (Airgas, 99.999%) through separate 10 mm diameter glass capillary arrays directed at the cooled wafer. Partial pressures of each ice component were maintained at 2 × 10⁻⁸ Torr during ice deposition by the use of leak valves. Ice thickness was determined to be 750 ± 50 nm by monitoring the ice deposition with a helium-neon laser (CVI Melles-Griot, 25-LHP-230, 632.8 nm) at a 4° angle of incidence and measuring variations in reflected power due to thin film interference by the

Table 1
Experimental Parameters of the Ices: Composition, Thickness, Irradiation Dose, and Photon Energies

	Composition	Ratio	Thickness (nm)	Current (nA)	Time (s)	Dose, Methanol (eV molecule ⁻¹)	Dose, Carbon Dioxide (eV molecule ⁻¹)	Photon Energy (eV)
1	CH ₃ OH:CO ₂	1.3 ± 0.5 : 1	750 ± 50	0	0	0	0	11.10
2	CH ₃ OH:CO ₂	1.2 ± 0.5 : 1	750 ± 50	18 ± 1	15.0 ± 0.1	0.45 ± 0.05	0.58 ± 0.06	11.10
3	CH ₃ OH:CO ₂	1.1 ± 0.4 : 1	750 ± 50	49 ± 1	30.0 ± 0.1	2.3 ± 0.2	3.2 ± 0.3	11.10
4	¹³ CH ₃ OH: ¹³ CO ₂	1.3 ± 0.1 : 1	750 ± 50	20 ± 1	15.0 ± 0.1	0.48 ± 0.05	0.66 ± 0.07	11.10
5	¹³ CH ₃ OH: ¹³ CO ₂	1.6 ± 0.8 : 1	750 ± 50	49 ± 1	30.0 ± 0.1	2.4 ± 0.2	3.2 ± 0.3	11.10
6	CD ₃ OD:CO ₂	2.5 ± 0.4 : 1	750 ± 50	20 ± 1	15.0 ± 0.1	0.57 ± 0.6	0.69 ± 0.07	11.10
7	CD ₃ OD:CO ₂	2.5 ± 0.7 : 1	750 ± 50	49 ± 1	30.0 ± 0.1	2.8 ± 0.2	3.5 ± 0.3	11.10
8	CH ₃ OH:CO ₂	1.1 ± 0.5 : 1	750 ± 50	19 ± 1	15.0 ± 0.1	0.54 ± 0.06	0.66 ± 0.08	10.56
9	CH ₃ OH:CO ₂	1.1 ± 0.6 : 1	750 ± 50	50 ± 1	30.0 ± 0.1	2.9 ± 0.3	3.6 ± 0.3	10.56
10	CH ₃ OH:CO ₂	1.0 ± 0.4 : 1	750 ± 50	19 ± 1	15.0 ± 0.1	0.44 ± 0.05	0.61 ± 0.06	9.93
11	CH ₃ OH:CO ₂	0.7 ± 0.4 : 1	750 ± 50	50 ± 1	30.0 ± 0.1	2.9 ± 0.3	3.5 ± 0.4	9.93
12	CH ₃ OH:CO ₂	1.9 ± 0.8 : 1	750 ± 50	20 ± 1	15.0 ± 0.1	0.47 ± 0.05	0.65 ± 0.06	9.73
13	CH ₃ OH:CO ₂	0.8 ± 0.4 : 1	750 ± 50	96 ± 1	60.0 ± 0.1	11 ± 1	14 ± 1	8.76

Table 2
Parameters Used in Dosage Calculation and Resulting Doses

Irradiated area	1.6 ± 0.1 cm ²		
Initial kinetic energy of e ⁻	5.000 keV		
Irradiation current	20 ± 1 nA		
Total number of e ⁻	(1.01 ± 0.06) × 10 ¹⁴		
Average energy of backscattered e ⁻	3.342 keV		
Fraction of backscattered e ⁻	0.36		
Average energy of transmitted e ⁻	0.000 keV		
Fraction of Transmitted e ⁻	0.00		
Total molecules irradiated	7.64 × 10 ¹⁷		
Ice composition	methanol-carbon dioxide	methanol-d ₄ -carbon dioxide	methanol- ¹³ C-carbon dioxide- ¹³ C
Density of mixed ice	0.945 g cm ⁻³	0.993 g cm ⁻³	0.969 g cm ⁻³
Average penetration depth	320 ± 30 nm	274 ± 30 nm	308 ± 30 nm
Dose per molecule of methanol	0.45 ± 0.05	0.57 ± 0.6	0.48 ± 0.05
Dose per molecule of carbon dioxide	0.58 ± 0.06	0.69 ± 0.07	0.66 ± 0.07

ice (Turner et al. 2015). An index of refraction, necessary to determine thickness from interferometric measurements, was approximated to be 1.28 ± 0.02 by the average of the indexes of refraction of the two components, 1.27 ± 0.02 for carbon dioxide at 20–25 K (Bouilloud et al. 2015) and 1.296 at 15 K for methanol (Hudson et al. 2020). Fourier transform infrared (FTIR) spectra (Thermo Electron, Nicolet 6700) were measured in the range of 6000–500 cm⁻¹ after ice deposition at 5.0 ± 0.2 K and used to calculate the relative abundance of the two components. Relative concentrations of methanol and carbon dioxide in ices were determined using integrated infrared absorptions ν_1 (3600–2700 cm⁻¹, 1.01×10^{-16} cm molecule⁻¹) and ν_8 (1031 cm⁻¹, 1.07×10^{-17} cm molecule⁻¹) for methanol and $\nu_1 + \nu_3$ (3708 cm⁻¹, 1.8×10^{-18} cm molecule⁻¹), $2\nu_2 + \nu_3$ (3600 cm⁻¹, 5.5×10^{-19} cm molecule⁻¹), and ν_3 (¹³CO₂; 2283 cm⁻¹, 6.8×10^{-17} cm molecule⁻¹) for carbon dioxide on the basis of band positions and absorption coefficients compiled by Bouilloud et al. (2015).

After deposition, ices were irradiated with 5 keV electrons (SPECS, EQ PU-22) with varying currents and times as listed

in Table 1 over an area of 160 mm² at a 70° angle of incidence. These electrons simulate secondary electrons produced in the track of GCRs. An average penetration depth of 320 ± 30 nm was determined for ices without isotopic labeling with the aid of Monte Carlo simulations (CASINO 2.42, Drouin et al. 2007) using the parameters detailed in Table 2. For the purposes of the simulation the average density of the ice components, 0.779 g cm⁻³ at 15 K for methanol (Hudson et al. 2020) and 1.11 ± 0.03 g cm⁻³ for carbon dioxide at 25 K (Bouilloud et al. 2015), was used as an approximation for the unknown density of the mixed ices. Variations in density due to isotopic labeling were taken into account. The average penetration depth is significantly less than the ice thickness (750 ± 50 nm) by design to prevent energetic electron-initiated interactions between the ice and the silver substrate (Drouin et al. 2007). Energetic doses reported in Table 1 represent the calculated total absorbed dose averaged over all molecules between the ice surface and the average penetration depth. Irradiation doses administered to the studied ices correspond to 10⁶ to 10⁷ yr of exposure to a molecular cloud environment. FTIR spectra were

measured during and after irradiation to verify changes in the spectrum due to reactions and to determine new functional groups and smaller species produced.

The photoionization reflectron time-of-flight mass spectrometry (PI-ReToF-MS) technique utilized in this research has been discussed in detail previously (Abplanalp et al. 2016a). Ices were heated to 320 K with TPD at a rate of 0.5 K min⁻¹. During TPD, pulsed 30 Hz coherent vacuum ultraviolet (VUV) light was passed 2 mm above the surface of the ice to photoionize subliming molecules. VUV light was produced via several resonant four-wave mixing ($\omega_{\text{VUV}} = 2\omega_1 \pm \omega_2$) schemes. Sum frequency generation ($2\omega_1 + \omega_2$) with the 249.6 nm (ω_1 ; dye laser, Sirah Lasertechnik, Cobra-Stretch) two-photon absorption of Xenon and 1064 nm (ω_2 ; Nd:YAG laser, Spectra-Physics, Quanta Ray PRO 270-30) was used to produce 11.10 eV photons. Difference frequency generation ($2\omega_1 - \omega_2$) with 202.3 nm (ω_1) and a second dye laser operating at 730.8 or 490.7 nm (ω_2) produced photons at 10.56 or 9.73 eV, respectively. Alternatively, exploiting the same two-photon absorption and Nd:YAG harmonics at 532 or 355 nm produced photons of 9.93 or 8.76 eV. After generation of the selected ω_1 and ω_2 , the lasers were made collinear and directed through a lens (Thorlabs, LA5479, $f = 300$ mm) and focused into a jet of rare gas in the VUV generation vacuum chamber. Coherent VUV light exiting this chamber was separated from ω_1 and ω_2 by passing the collinear beams through an off-axis lithium fluoride (LiF) biconvex lens (Korth Kristalle, $R_1 = R_2 = 131.22$ mm), which imparts an angular separation between the three frequencies and directs only the VUV light through an aperture to the ionization region. Ions formed are mass-analyzed in a ReToF-MS (Jordan TOF Products) and detected with a dual microchannel plate (MCP) detector in the chevron configuration (Jordan TOF Products). The MCP signal was amplified (Ortec, 9305) before discrimination and amplification to 4 V (Advanced Research Instruments Corp., F100-TD) and ultimately recorded by a multichannel scaler (FAST ComTec, MCS6A) interfaced to a personal computer. Ion arrival times were recorded to 3.2 ns accuracy, mass spectra were repeated at a rate of 30 Hz, and new mass spectra were accumulated every 2 minutes during TPD until the temperature of the sample reached 320 K.

2.2. Computational Methods

Geometries of neutral molecules were optimized for all possible combinations of dihedral angles of asymmetric internal rotors, e.g., -OH, -CHO, -COOH, -CR¹R²R³, where at least one R^{*i*} is unique. For ions, starting geometries were taken from the optimized neutral molecules. Molecular parameters of both neutral and cationic states of each conformer were optimized using density functional theory with the B3LYP hybrid functional and the 6-311G(2d,d,p) (CBSB7) basis set, which provide a chemical accuracy 0.01–0.02 Å for bond lengths as well as 1°–2° for bond angles. The energies were computed with the composite CBS-QB3 level (Montgomery et al. 1999, 2000) of theory, which is characterized by the mean absolute error of 4.52 kJ mol⁻¹ and rms error of 6.32 kJ mol⁻¹ for computed enthalpies of formation for the G2/97 test set. This method also has a mean absolute error of 0.05 eV for computed adiabatic ionization energies, which has been applied as ± 0.05 eV to all conformer-specific ionization energies that form the ranges presented in

Figure 1. The GAUSSIAN 09 program package (Frisch et al. 2009) was utilized for all calculations.

3. Results

3.1. FTIR Analysis

FTIR spectra of methanol-carbon dioxide ices were collected before and after irradiation with energetic electrons (Figure 2, Table 3). Several new absorptions were detected that result from reactions that took place during the irradiation. New alcohols formed are expected to exhibit OH stretching centered at 3300 cm⁻¹ where the methanol OH stretch is dominant. The intensity of the methanol OH stretch was found to decrease above 3250 cm⁻¹ while a broad increase in absorption was observed in the range of 3250–2400 cm⁻¹. Both the position and width of this increased absorption matched the expected range for OH stretching modes in carboxylic acids (RCOOH) participating in hydrogen bonding (Socrates 2004). The range of increased absorption also included the CH stretching region 3000–2800 cm⁻¹ (Socrates 2004). The asymmetric CO stretch of carbon dioxide (ν_3) at 2343 cm⁻¹ lies well outside of the C=O stretching region of carbonyl-containing organic molecules (1850–1550 cm⁻¹), as a result this region of the spectrum is unobstructed by absorption from the reactants. Carbon monoxide (CO) was identified as a product by its well-known absorption at 2136 cm⁻¹. Deconvolution of the CO stretching region into discrete Gaussian peaks (Figure 2(C)) shows at least three separate absorptions. The highest frequency peak in this region at 1773 cm⁻¹ is not assigned to a specific molecule but is likely due to the formation of one or more carbonyl (C=O) containing species. In methanol-d₄-carbon dioxide ice this peak is found to be significantly more intense and may indicate an isotopic effect on the formation of deuterated carbonyl-containing molecules. The central of the three CO stretching peaks at 1722 cm⁻¹ is assigned to ν_2 of formaldehyde (H₂CO) produced during irradiation (Butscher et al. 2016). This peak is both more intense than the other peaks in the CO stretching region and can therefore be identified in deuterium and ¹³C ices with redshifts of 29 and 37 cm⁻¹, respectively (Figures 3 and 4, Table 3). CH stretches from formaldehyde and other aldehydes (RCHO) and ketones (RC(O)R') must be present as well but are not observed as discrete absorptions. These vibrations are likely contributors to the broad increase observed in the OH/CH stretching regions. The third peak in the CO stretching region at 1653 cm⁻¹ is tentatively assigned to a hydrogen-bonding carboxylic acid, which is reported to exhibit CO stretching frequencies in the range of 1680–1650 cm⁻¹ (Socrates 2004). Lastly, the formation of methane during irradiation was confirmed by the presence of its asymmetric deformation (ν_4) at 1292 cm⁻¹.

Both *cis*- and *trans*-hydroxycarbonyl radical (HOĈO) have been detected in CO matrix isolation by Milligan & Jacox (1971), and have OH stretches reported at 3312 and 3456 cm⁻¹, respectively. These absorptions are not detected here, though they would overlap with the much stronger OH stretch of methanol, which may obstruct their detection. The C=O stretch of *cis*- and *trans*-hydroxycarbonyl are reported 1797 and 1833 cm⁻¹, respectively, and have been observed in apolar methane-carbon dioxide ices at 1823 and 1842 cm⁻¹ (Kleimeier & Kaiser 2022). However, no new absorptions are observed above 1800 cm⁻¹ in Figure 2(C), it is possible that the absorption seen at 1773 cm⁻¹ after deconvolution is

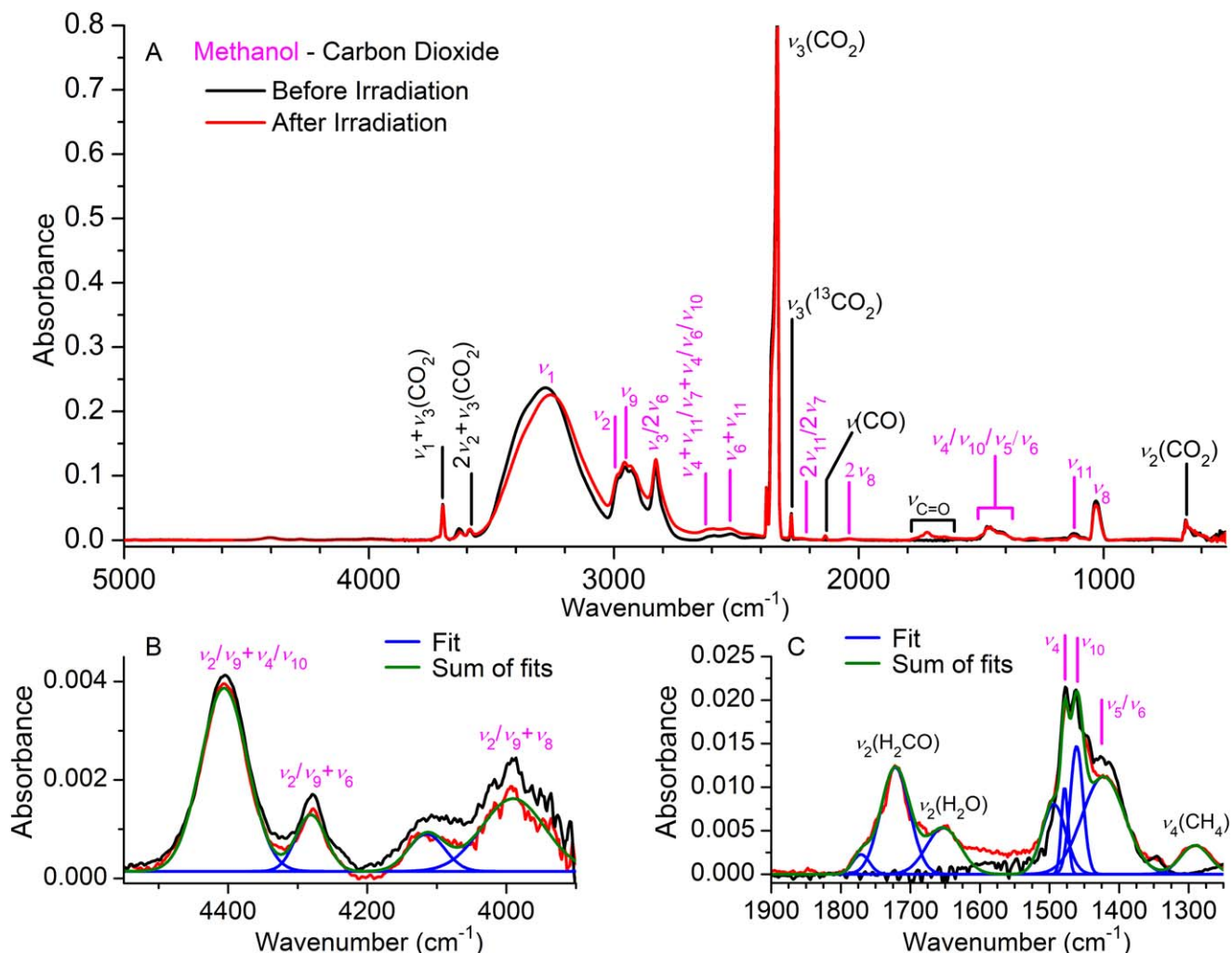


Figure 2. Infrared spectra of methanol-carbon dioxide ice before (black) and after (red) irradiation with assignments given in Table 1, with magnified views and deconvolution of the regions (B) 4550–3900 cm^{-1} and (C) 1900–1350 cm^{-1} .

hydroxycarbonyl though this 20 cm^{-1} lower than its observation in CO ice. It is also possible that the lifetime of hydroxycarbonyl is limited by reactions or the polarity of the ice such that its concentration is below the limit of detectability. The presence of CH and CO stretching features attributable to carboxylic acids shows that while the hydroxycarbonyl radical ($\text{HO}\dot{\text{C}}\text{O}$) is not detected directly via infrared spectroscopy its presence is implied due to absorptions in the infrared that can be linked to vibrational modes of carboxylic acids, which are expected to form by radical recombination of most radicals with hydroxycarbonyl. While these results are useful in verifying the extent of irradiation and identifying the presence of new *functional groups* including carboxylic acids, this information alone is insufficient for identifying complex molecules formed in the ice. To identify the presence, or lack thereof, of isomers shown in Figure 1 isomer-selective techniques must be employed in the form of mass spectrometry with tunable photoionization.

3.2. PI-ReToF-MS Analysis

PI-ReToF-MS was used in these experiments to detect and analyze molecules during sublimation. A species can only be detected when the employed photon energy is greater than its adiabatic ionization energy (Abplanalp et al. 2015;

Kostko et al. 2016; Eckhardt et al. 2019; Abplanalp et al. 2019). Selected mass spectra measured during the course of this investigation are plotted as a function of temperature in Figure 5. A mass spectrum during TPD was measured without prior irradiation (Figure 5(A)) in which no ions with $m/z = 76$ ($\text{C}_2\text{H}_4\text{O}_3$) were detected, ensuring that subsequent experiments would be unaffected by background signal. The IEs shown in Figure 1 are the result of high-quality CBS-QB3 calculations and account for changes in IE due to conformational changes, and these values are also corrected for the Stark effect of the mass spectrometer acceleration field, which can reduce effective IEs by up to 0.03 eV (Zhu et al. 2019). These IEs show that the first-generation products carbonic acid monomethyl ester (1, IE = 10.62–10.96 eV) and glycolic acid (2, IE = 10.00–10.54 eV) have no overlap in their possible IEs and can be readily distinguished with this technique. Additionally, second-generation products ethenetriol (3, IE = 7.72–8.03 eV) and dihydroxyacetaldehyde (4, IE = 8.92–9.83 eV) are similarly identifiable due to differences between their IEs. Given the reaction mechanism outlined in Figure 1, decomposition followed by radical-radical recombination, it is not expected that any other possible isomers of $\text{C}_2\text{H}_4\text{O}_3$ will form during irradiation with the modest irradiation doses employed. Though other radicals such as methyl (CH_3), hydroxyl (OH),

Table 3
Infrared Absorption Features Observed in the Studied Ices

Methanol–Carbon Dioxide	Methanol-d ₄ –Carbon Dioxide	Methanol- ¹³ C–Carbon Dioxide- ¹³ C	Assignment ^{a,b}
Wavenumber (cm ⁻¹)	Wavenumber (cm ⁻¹)	Wavenumber (cm ⁻¹)	
Infrared absorptions observed before irradiation			
4406		4390	$\nu_1/\nu_9 + \nu_4/\nu_{10}$ (CH ₃ OH)
4280		4278	$\nu_2/\nu_9 + \nu_6$ (CH ₃ OH)
3992		3962	$\nu_2/\nu_9 + \nu_8$ (CH ₃ OH)
3698	3700	3641	$\nu_1 + \nu_3$ (CO ₂)
3588	3593	3620	$2\nu_2 + \nu_3$ (CO ₂)
3250	2450	3292	ν_1 (CH ₃ OH)
2986	2247	2952	ν_2 (CH ₃ OH)
2953	2220	2922	ν_9 (CH ₃ OH)
3780	2075	2828	$\nu_3/2\nu_6$ (CH ₃ OH)
2592			$\nu_4 + \nu_{11}/\nu_9 + \nu_7/\nu_6/\nu_{10}$ (CH ₃ OH)
2521		2502	$\nu_6 + \nu_{11}$ (CH ₃ OH)
2343	2344	2346	ν_3 (CO ₂)
2276	2277	2279	ν_3 (¹³ CO ₂)
2231	1923		$2\nu_{11}/2\nu_7$ (CH ₃ OH)
2036			$2\nu_8$ (CH ₃ OH)
1477	1132–1080	1476	ν_4 (CH ₃ OH)
1461	1132–1080	1460	ν_{10} (CH ₃ OH)
1447	1132–1080	1439	ν_5 (CH ₃ OH)
1415	1064	1417	ν_6 (CH ₃ OH)
1123	974	1113	ν_{11} (CH ₃ OH)
	900		ν_7 (CH ₃ OH)
1031	802	1011	ν_8 (CH ₃ OH)
664	667	647	ν_2 (CO ₂)
Infrared absorptions observed after irradiation			
3250–2400	3250–2500	2380–1900	CH stretch
2136	2139	2089	ν (CO)
1722	1693	1685	ν_2 (H ₂ CO) ^b
1773, 1653	1725, 1632	1643	C=O stretch
1652	1638	1642	ν_2 (H ₂ O) ^b
	1225		ν_2 (D ₂ O) ^c
1292		1270	ν_4 (CH ₄)

Notes.^a Assignments from Zhu et al. (2020b).^b Assignments from Bouilloud et al. (2015).^c Assignment from Zheng et al. (2007).

and carbon monoxide (CO) should form and undergo recombination, products of these reactions would have neither the same molecular formula nor mass.

The TPD profiles observed for $m/z = 76$ observed with 11.10 eV photoionization for methanol–carbon dioxide ices and two different irradiation doses ((A) and (B)) are shown in

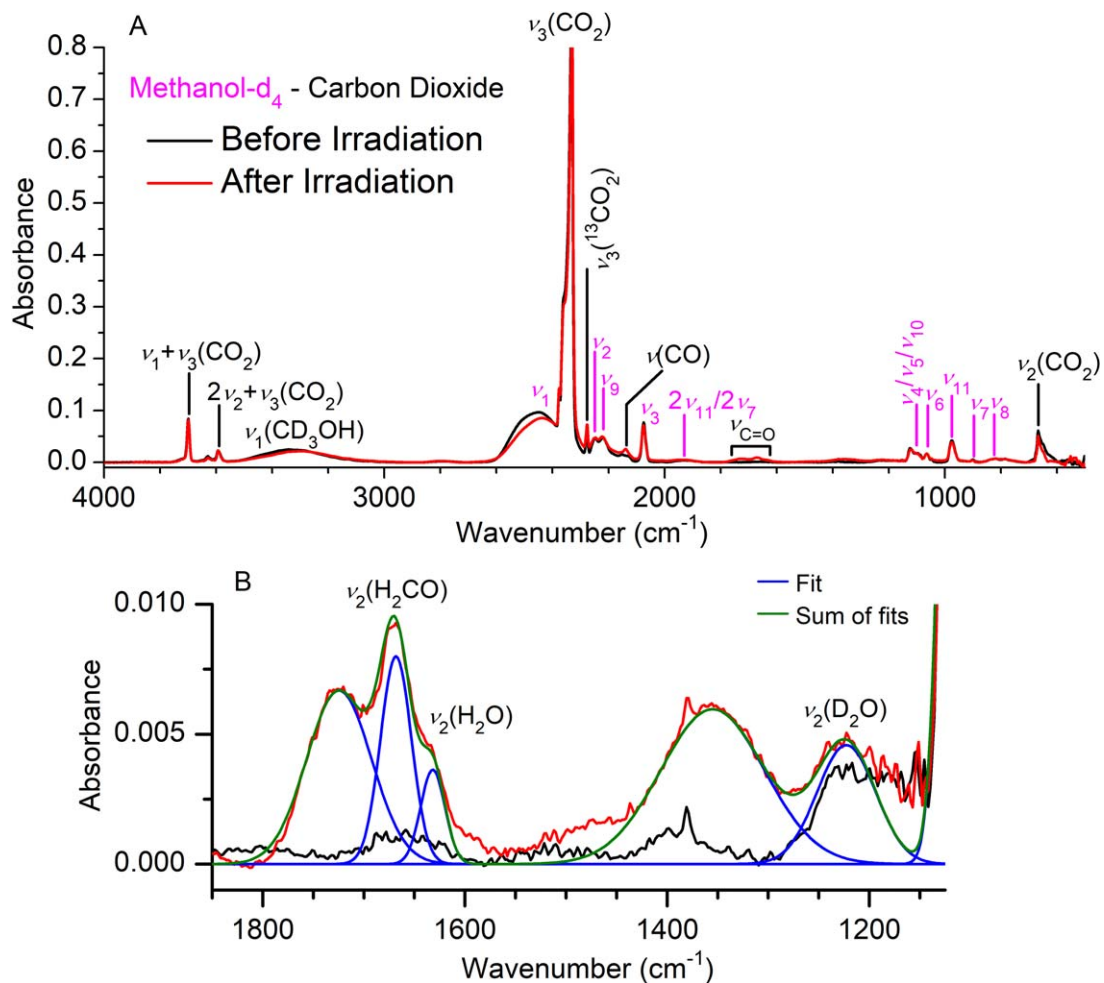


Figure 3. Infrared spectra of (A) methanol- d_4 -carbon dioxide ice before (black) and after (red) irradiation with (B) a magnified and deconvoluted view for the region 1850–1150 cm^{-1} .

Figure 6. The TPD profiles observed with a dose of 0.45 ± 0.05 eV for methanol and 0.58 ± 0.06 eV for carbon dioxide, 0.48 ± 0.05 eV for methanol- ^{13}C and 0.66 ± 0.07 eV for carbon dioxide- ^{13}C , 0.57 ± 0.6 eV for methanol- d_4 and 0.69 ± 0.07 eV for carbon dioxide (experiments 2, 4, and 6 in Table 1, respectively) are shown in (A). The bimodal profile for all three isotopically labeled ices with lower doses show peaks at about 195 and 247 K. This is consistent with the presence of two isomers with different sublimation temperatures and are likely caused by carbonic acid monomethyl ester (1) and glycolic acid (2). However, 11.10 eV photons can ionize all four isomers and ethenetriol (3) and dihydroxyacetaldehyde (4) may be present. The TPD profiles observed with a dose of 2.3 ± 0.2 eV for methanol and 3.2 ± 0.3 eV for carbon dioxide, 2.4 ± 0.2 eV for methanol- ^{13}C and 3.2 ± 0.3 eV for carbon dioxide- ^{13}C , 2.8 ± 0.2 eV for methanol- d_4 and 3.5 ± 0.3 eV for carbon dioxide (experiments 3, 5, and 7 in Table 1) are shown in (B). With these larger doses the bimodal profile seen with lower doses is observed again with all isotopically labeled ices exhibiting peaks at about 204 and 251 K. The repetition of this pattern shows that whichever isomers are formed with exposure to the lower dose are still formed with similar, though not identical, relative intensity despite changes in dose, and no new isomers with significantly different sublimation temperature are formed with detectable intensity relative to the two peaks observed.

The peaks observed in Figure 6 were deconvoluted by fitting to split Pearson VII distributions for the methanol-carbon dioxide ices without isotopic labeling. For the peak at 195 K a total signal of 650 ± 200 counts was observed with a lower dose (Figure 6(A)) and 3200 ± 700 counts at higher dose (B). This shows that a fivefold increase in irradiation dose results in a proportional increase in ion signal, and this species is likely not undergoing decomposition at a significant rate and is stable in the 5 K ice. Furthermore, it appears that the limiting factor in its formation is reaction initiation provided by energetic electrons. Conversely, the peak at 247 K increases in intensity from 970 ± 200 counts to 2400 ± 500 and is found to be lower in relative intensity with a higher dose for all ices, regardless of isotopic substitution. This may indicate that this species is not as stable or it could decompose under electron irradiation at a rate competitive with its rate of formation. Overall, these findings reveal that two distinct isomers are responsible for both sublimation events.

Here, 11.10 eV photons are capable of photoionizing *all* four isomers that may be formed. However, 10.56 eV photons are not energetic enough to ionize carbonic acid monomethyl ester (1, IE = 10.62–10.96 eV). A photon energy of 9.73 eV is substantially below the predicted adiabatic IEs of carbonic acid monomethyl ester (1) and glycolic acid (2, IE = 10.00–10.54 eV). Neither of these first-generation products can be ionized at 9.73 eV but second-generation products ethenetriol (3,

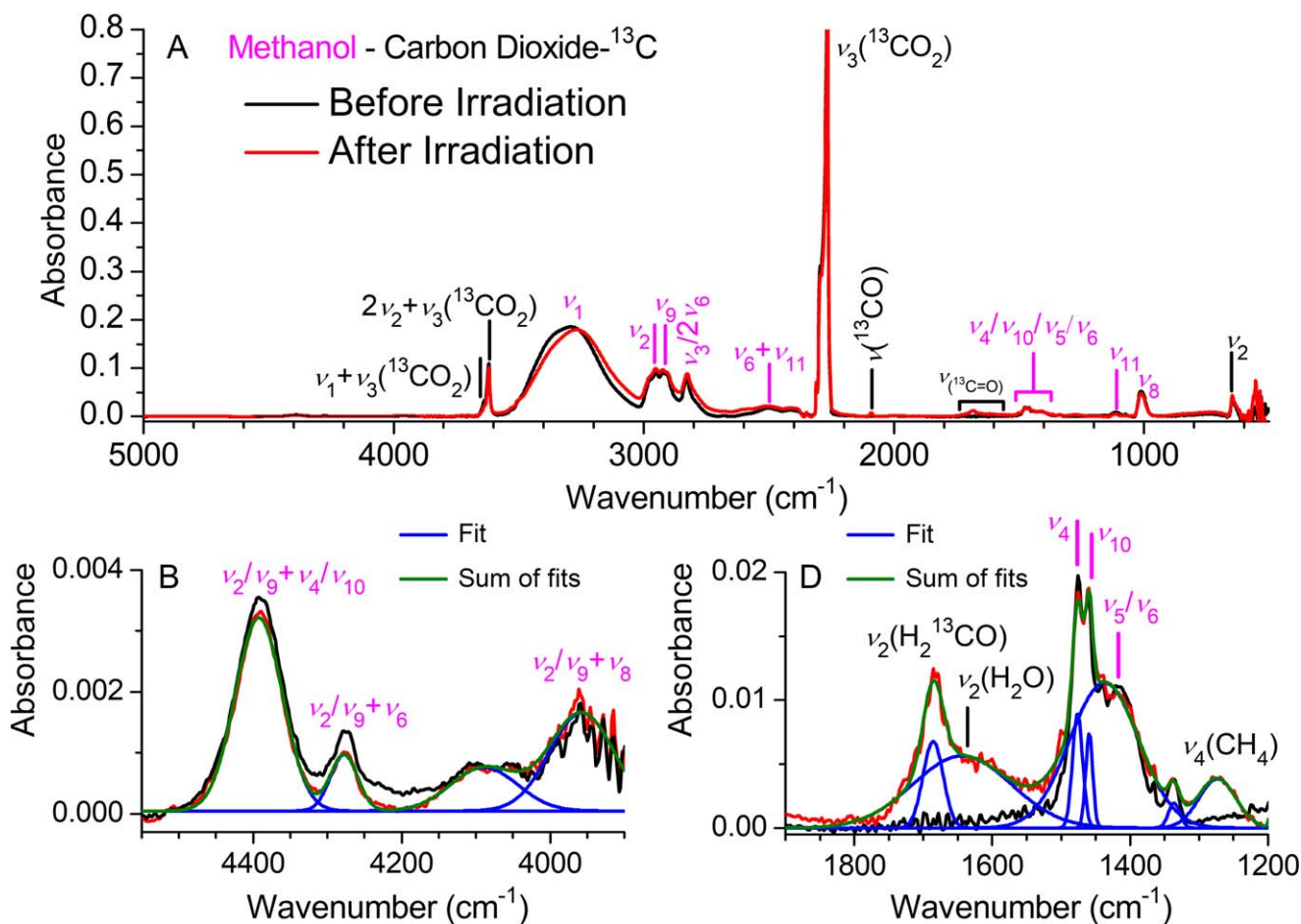


Figure 4. Infrared spectra of (A) methanol- d_4 -carbon dioxide and (B) methanol- ^{13}C -carbon dioxide- ^{13}C ices before (black) and after (red) irradiation with magnified views and deconvolution for the regions (B) 4550–3900 cm^{-1} and (C) 1900–1200 cm^{-1} .

IE = 7.72–8.03 eV) and dihydroxyacetaldehyde (4, IE = 8.92–9.83 eV) may be observable if present. Additionally, photoionization at 9.93 eV was investigated, while closer to the possible IE of glycolic acid (2) this photon energy is above the range of IEs possible for dihydroxyacetaldehyde (4). Figure 7 shows how the two peaks observed in Figure 6 responded to variation in VUV photon energy. While both peaks are observed with 11.10 eV photons, the lower temperature peak is not present when a photon energy of 10.56 eV is employed. This sublimation event at 195 K (Figure 7(A)) can then be linked to the presence of carbonic acid monomethyl ester (1). With photon energy of 9.73 eV, 0.27 eV below the range of possible adiabatic IEs for any conformer of glycolic acid, the higher temperature peak is also not observed. This observation was repeated at 9.93 eV to confirm that no signal can be attributed to the presence of any high-energy conformers of dihydroxyacetaldehyde (4). Because no ion signal is detected at 9.73 or 9.93 eV, the sublimation event at 247 K (Figure 7(A)) must represent a molecule with an ionization energy between 10.56 and 9.93 eV, and can only be glycolic acid (2).

For investigating the formation of carbonic acid monomethyl ester (1) and glycolic acid (2), lower irradiation doses were employed and shown in Figure 7(A). Ices were then subjected to higher doses to investigate the possible formation of tautomers ethenetriol (3) and dihydroxyacetaldehyde (4), and these experiments are shown in Figure 6(B) and Figure 7(B). With irradiation doses of about $2.3 \pm 0.2 \text{ eV molecule}^{-1}$ for

methanol and $3.2 \pm 0.3 \text{ eV molecule}^{-1}$ for carbon dioxide, photoionization at 11.10, 10.56, and 9.93 eV show the same response to changes in photon energy that was used to identify the presence of carbonic acid monomethyl ester (1) and glycolic acid (2) above (Figure 7(A)). Photoionization at 9.93 eV should be able to ionize ethenetriol (3) and dihydroxyacetaldehyde (4); however, no ions with $m/z = 76$ are detected with this photon energy. In an effort to increase the abundance of glycolic acid (2) and further promote tautomerization, the dosage was increased to $11 \pm 1 \text{ eV molecule}^{-1}$ for methanol and $14 \pm 1 \text{ eV molecule}^{-1}$ for carbon dioxide. Photoionization at 8.76 eV was employed with this increased dose because the VUV generation system was capable of producing nearly twice the photon flux at this energy compared to 9.93 eV, thus increasing the sensitivity of the apparatus while still using photons with energy substantially in excess of the predicted adiabatic IE of ethenetriol (3). The result of this experiment, shown in Figure 7(B), confirms that ethenetriol (3) was either not formed or is present in such low quantities as to be undetectable.

4. Discussion

The results discussed above demonstrate that COMs containing a carboxylic acid functional group can be formed under astrophysical conditions in mixed ices containing carbon dioxide (CO_2) and a source of atomic hydrogen (H). Initially, Reactions (1)–(3) decompose methanol (CH_3OH) into methoxy

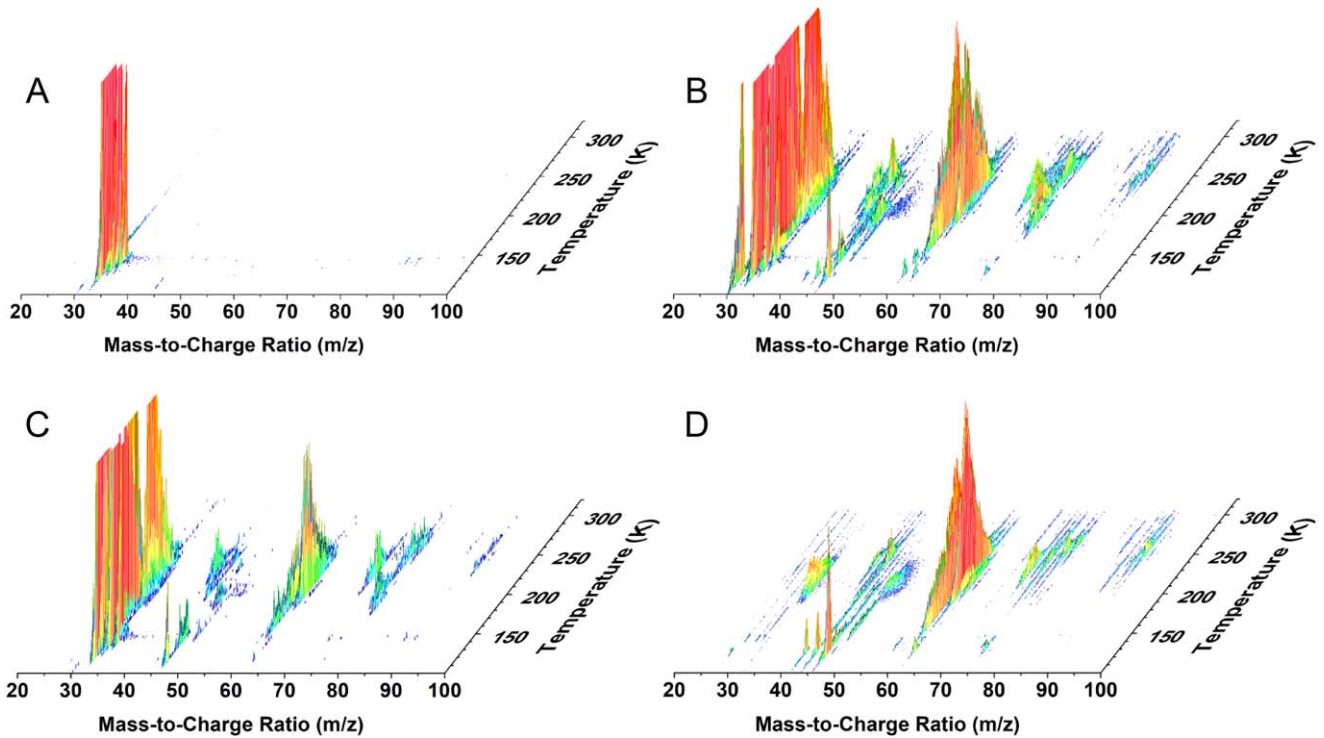
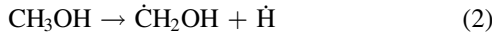
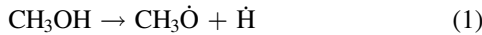
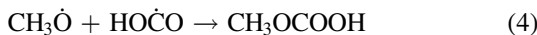


Figure 5. Temperature-dependent photoionization mass spectra of irradiated methanol-carbon dioxide ices as a function of temperature during TPD: (A) without irradiation at a photon energy of 11.10 eV, (B) an irradiation dose of 2.3 ± 0.2 eV molecule⁻¹ for methanol and 3.2 ± 0.3 eV molecule⁻¹ for carbon dioxide and photon energy of 11.10 eV, (C) 0.45 ± 0.05 eV molecule⁻¹ for methanol and 0.58 ± 0.06 eV molecule⁻¹ for carbon dioxide and photon energy of 11.10 eV, and (D) 2.9 ± 0.3 eV molecule⁻¹ for methanol and 3.6 ± 0.3 eV molecule⁻¹ for carbon dioxide and photon energy of 10.56 eV.

(CH₃Ö, Reaction (1)) and hydroxymethyl (Ĉ₂OH, Reaction (2)) radicals (Zhu et al. 2019), and result in the formation of hydroxycarbonyl radical (HOĈO, Reaction (3)) upon the interaction of carbon dioxide (CO₂) with atomic hydrogen (Ĥ) liberated during the decomposition of methanol (Kleimeier & Kaiser 2022).



Because these reactions are strongly endoergic by 218.8 ± 0.3 kJ mol⁻¹ for Reaction (1) and 200.5 ± 0.3 kJ mol⁻¹ for Reaction (2) (Ruscic & Bross 2021), the input of energy originating from GCRs is necessary for initiation. The hydroxycarbonyl radical can lead to the formation of formic acid (HCOOH) after recombination with atomic hydrogen and serves as an intermediate in the formation of a diverse range of carboxylic acids, e.g., glyoxylic acid (Turner et al. 2021) and benzoic acid (McMurtry et al. 2016). These nonequilibrium reactions cannot occur in cold interstellar ices without an external source of energy. Subsequent reactions to form the first-generation products carbonic acid monomethyl ester (1) and glycolic acid (2) rely on barrierless radical-radical recombination of hydroxycarbonyl radical with methoxy (Reaction (4)) or hydroxymethyl (Reaction (5)) radicals, respectively.



Subsequent reactions relevant to this investigation require the input of additional energy to induce tautomerization, a specific class of isomerization. Carbonic acid monomethyl ester (1) has no carbon-carbon bonds and cannot tautomerize, while glycolic acid (2) has the requisite carbon-carbon bond adjacent to a hydroxyl group (-OH) and can tautomerize to an enol, ethenetriol (3), which in turn can tautomerize to an alternative keto form, dihydroxyacetaldehyde (4), via Reactions (6) and (7).



Furthermore, it is possible that hydrogen transfer between the hydroxyl (-OH) and carboxyl (-COOH) groups of glycolic acid through a 5-membered cyclic shared-proton transition state can allow direct isomerization of glycolic acid (2) to dihydroxyacetaldehyde (4) (Reaction (8)).



Reactions (6)–(8) are not radical recombination and are not barrierless, but require the input of further energy from the GCR proxy to surmount the barrier imposed by hydrogen transfer. Because of the joint need for additional energy to overcome a reaction barrier and prior formation of glycolaldehyde (2), similar tautomerization reactions have been observed previously only after larger energetic doses. Previous investigations have shown enol formation from acetaldehyde (CH₃CHO) (Kleimeier & Kaiser 2021), acetic acid (CH₃COOH) (Kleimeier & Kaiser 2022), glycolaldehyde (HOCH₂CHO) (Kleimeier et al. 2021), propanal (CH₃CH₂CHO) (Abplanalp et al. 2016b), and pyruvic

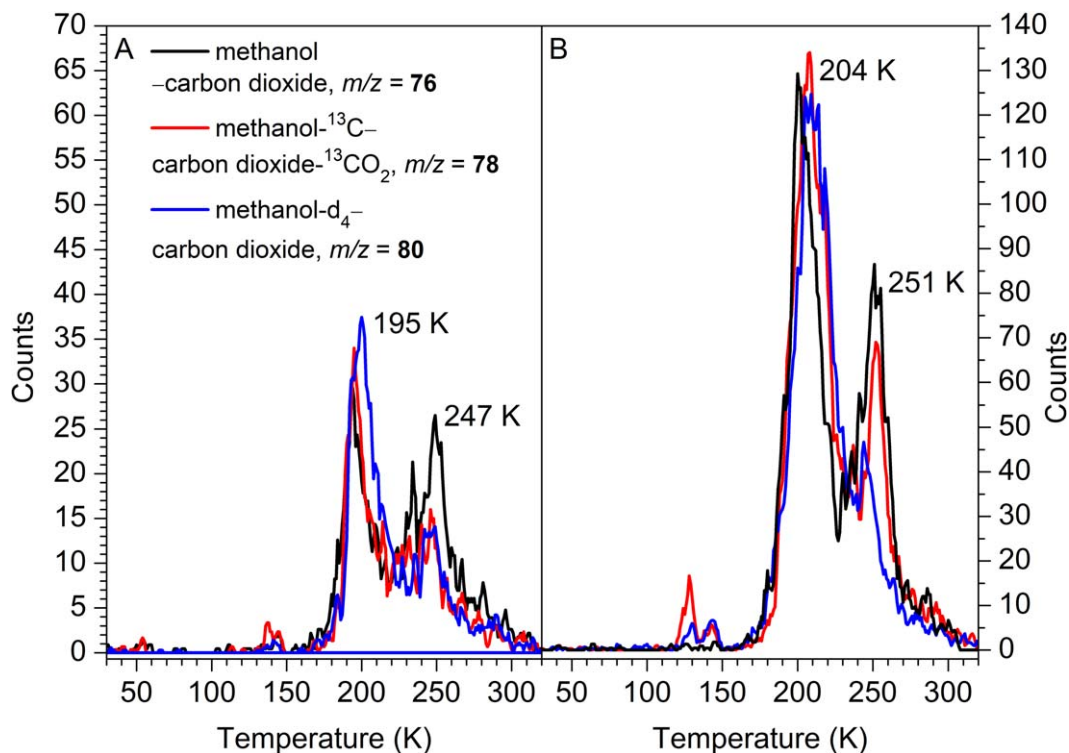


Figure 6. Temperature-dependent sublimation profiles of $C_2H_4O_3$ isomers along with their isotopic substituted counterparts observed with methanol-carbon dioxide ice, methanol- ^{13}C -carbon dioxide- ^{13}C , and methanol- d_4 -carbon dioxide ices at the indicated mass-to-charge ratio (m/z) after irradiation with (A) a dose of about $0.4\text{--}0.6\text{ eV molecule}^{-1}$ for methanol and $0.5\text{--}0.7\text{ eV molecule}^{-1}$ for carbon dioxide or (B) a dose of $2.3\text{--}2.9\text{ eV molecule}^{-1}$ for methanol and $3.2\text{--}3.6\text{ eV molecule}^{-1}$ for carbon dioxide.

acid ($CH_3COCOOH$) (Kleimeier et al. 2020) by exposure to similarly large doses. However, here we employ doses up to what a molecule may experience during the entire life of a molecular cloud and observe no evidence of any product of tautomerization. It is possible that these molecules cannot be formed via tautomerization in this simulated astrophysical environment or the polar ices studied here.

5. Astrophysical Implications

Our results provide evidence that highly oxygenated COMs can form on icy interstellar grains from precursors that are known to be abundant in molecular clouds, methanol (CH_3OH), and carbon dioxide (CO_2). Moreover, the reactions and products studied here are found to occur after irradiation with doses that are small in comparison to doses experienced by molecules during the lifetime of studied molecular clouds. Products were observed with substantial ion signal after exposure to doses as low as $0.45\text{ eV molecule}^{-1}$ for methanol and $0.58\text{ eV molecule}^{-1}$ for carbon dioxide, approximately 1%–10% of the total irradiation experienced by molecules over the lifetime of a molecular cloud (Yeghikyan 2011). The observation of carbonic acid monomethyl ester (1) shows for the first time that a carbonic ester, in this case, a hemiester, can form in this astrophysically relevant environment from molecules that are common in interstellar ices. This prebiotic molecule’s reactivity has led to difficulty in its formation and observation in laboratory settings, and this same reactivity can lead to further complex chemistry and the formation of increasingly large species via well-characterized condensation reactions. Glycolic acid (2) is also found to form during the irradiation of the same ice. This molecule is an active

component of photorespiration in plants where it aids in the production of sugar through photosynthesis and is cyclically converted into amino acids glycine and serine in turn (South et al. 2017).

Due to the abundance in interstellar ices of the reactants discussed here and the relatively low irradiation dose required for the reaction products to be observable, both carbonic acid monomethyl ester (1) and glycolic acid (2) are ideal candidates for identification via millimeter and submillimeter astronomy. Prior work on chemical modeling of interstellar ices suggests that these COMs may need to be formed by reactions of previously formed COMs such as aldehydes (Garrod et al. 2008); however, this is not found to be the case here where simple carbon dioxide (CO_2) and plentiful methanol (CH_3OH) are found to form these products directly. While these molecules may be formed in ices, the warming of these ices during star formation should allow them to enter the gas phase where they can be detected by their rotational spectra. The millimeter-wave spectrum of glycolic acid (2) has been measured by Kiesel et al. (2016) and is actively being searched for. Conversely, the rotational spectrum of carbonic acid monomethyl ester (1) has not been measured, though its gas-phase synthesis via pyrolysis of *tert*-butyl methyl carbonate ($(CH_3)_3COC(O)OCH_3$) has been demonstrated by Linden et al. (2018). Measurement of this heretofore unknown rotational spectrum of carbonic acid monomethyl ester (1) should be a fruitful next step in its eventual identification in the ISM.

The experiments at the University of Hawaii were supported by the US National Science Foundation (NSF), Division for Astronomy (NSF-AST 2103269). The W. M. Keck Foundation and the University of Hawaii at Manoa financed the

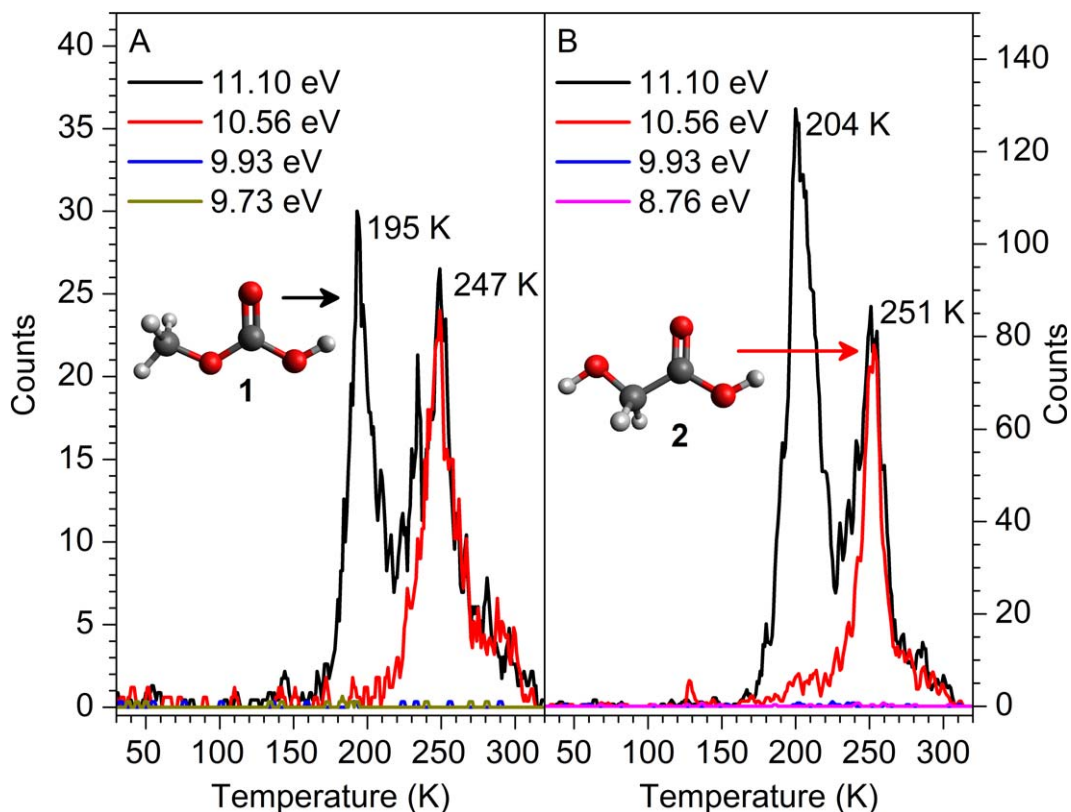


Figure 7. Temperature-dependent sublimation profiles of $C_2H_4O_3$ isomers observed with methanol–carbon dioxide ices at $m/z = 76$ after irradiation with (A) a dose of $0.4\text{--}0.6\text{ eV molecule}^{-1}$ for methanol and $0.5\text{--}0.7\text{ eV molecule}^{-1}$ for carbon dioxide and (B) a dose of at least $2.3\text{ eV molecule}^{-1}$ for methanol and $3.2\text{ eV molecule}^{-1}$ for carbon dioxide.

construction of the experimental setup. The electronic structure calculations were supported by the Ministry of Higher Education and Science of the Russian Federation via Grant 075-15-2021-597.

Appendix

Geometries, vibrational analyses, and zero-point corrections were calculated at the B3LYP/6-311(2d,d,p) level and are provided here in Table A1 with Cartesian coordinates

(Angstrom) and vibrational frequencies (wavenumbers, inverse centimeters) with intensities (kilometers per mole). The total, relative, and adiabatic ionization energies reported are calculated with the composite CBS-QB3 method and include B3LYP/6-311(2d,d,p) zero-point corrections. The cation isomer resulting from adiabatic ionization is indicated with ionization energy, the structures and energetics of which are listed in the latter part of the table. Conformers of each isomer are indicated by a letter and are listed in order of increasing relative energy.

Table A1
Computational Results for the Isomers of the C₂H₄O₃ Products in Figure 1

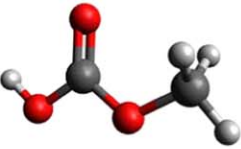
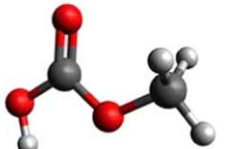
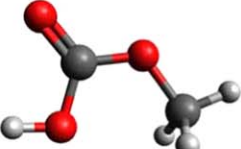
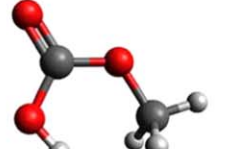
Isomer 1a				Isomer 1b			
							
Energy (hartree): -303.909842				Energy (hartree): -303.907886			
Relative energy (kJ mol ⁻¹): 0.0				Relative energy (kJ mol ⁻¹): 1.2			
Adiabatic IE (eV): 10.94 ± 0.05 (1c ⁺)				Adiabatic IE (eV): 10.88 ± 0.05 (1b ⁺)			
	x	y	z		z	y	z
C	-0.003777	0.113063	-0.005017	C	0.019098	0.089991	-0.029749
O	0.310954	-0.538135	1.238924	O	0.376825	-0.610843	1.176152
C	1.522820	-0.266004	1.724145	C	1.546207	-0.227818	1.738869
O	1.676606	-0.937670	2.879309	O	1.775814	-0.944913	2.850670
O	2.348715	0.454831	1.225759	O	2.280035	0.619612	1.324780
H	-1.010943	-0.213776	-0.252096	H	-0.931279	-0.336594	-0.342123
H	0.030711	1.197072	0.111557	H	-0.084895	1.157371	0.168492
H	0.699498	-0.187846	-0.782650	H	0.779588	-0.061882	-0.796558
H	2.560758	-0.716616	3.198477	H	1.043281	-1.562118	2.974951
Freq.	Int.	Freq.	Int.	Freq.	Int.	Freq.	Int.
107.814	0.431	1223.759	154.151	96.7709	1.4124	1216.225	0.4984
176.351	6.8594	1404.778	180.816	177.0861	5.2633	1344.479	608.632
296.054	10.1068	1484.029	65.876	290.8112	16.181	1477.51	47.2402
527.908	40.5537	1484.499	9.5974	514.1289	120.628	1483.018	9.565
550.875	107.022	1502.338	7.4431	528.013	1.4939	1503.191	9.096
670.38	2.1259	1831.775	400.759	674.1629	0.3904	1885.742	365.854
799.483	41.8269	3051.48	25.9114	786.1762	26.9111	3052.987	24.0052
912.487	18.3664	3124.255	22.4241	903.8319	54.3226	3127.485	20.6661
1096.27	7.0962	3161.4	15.2156	1087.23	37.0072	3160.126	15.1586
1178.45	0.9823	3813.993	94.5683	1177.826	0.5993	3800.191	74.8817
1212.54	385.574			1203.735	127.966		
Isomer 1c				Isomer 1d			
							
Energy (hartree): -303.904414				Energy (hartree): -303.893077			
Relative energy (kJ mol ⁻¹): 3.4				Relative energy (kJ mol ⁻¹): 10.5			
Adiabatic IE (eV): 10.78 ± 0.05 (1a ⁺)				Adiabatic IE (eV): 10.70 ± 0.05 (1d ⁺)			
	x	y	z		z	y	z
C	0.025005	0.033553	-0.020173	C	0.021645	0.023501	-0.024967
O	0.180897	-0.161203	1.398109	O	0.186646	-0.169230	1.380749

Table A1
(Continued)

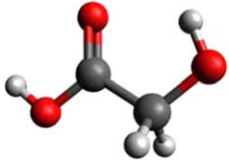
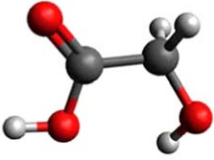
C	1.390741	-0.076474	1.953617	C	1.400529	-0.040487	1.979444
O	2.359525	0.198509	1.042219	O	2.445301	0.278647	1.178026
O	1.589240	-0.227556	3.125002	O	1.529240	-0.202028	3.150337
H	-1.039906	-0.087316	-0.205770	H	-1.035424	-0.139694	-0.223029
H	0.346874	1.033834	-0.312657	H	0.278273	1.045568	-0.325683
H	0.591522	-0.712192	-0.579307	H	0.600558	-0.705211	-0.603566
H	3.186199	0.238310	1.540226	H	2.192341	0.377669	0.254283
S1	Int.	Freq.	Int.	Freq.	Int.	Freq.	Int.
129.002	1.8809	1221.358	103.481	52.5764	5.4494	1208.587	30.5686
173.815	4.3973	1368.18	129.373	189.1335	1.9705	1304.645	461.683
315.632	2.5169	1490.091	8.7877	324.1782	0.6968	1480.825	13.5314
568.631	101.506	1493.594	17.9673	334.7964	98.9512	1501.005	16.0374
574.623	23.646	1499.078	28.7878	577.8161	5.2491	1503.246	8.6622
606.361	12.2717	1866.88	584.758	608.2252	5.375	1903.348	523.064
786.574	45.0501	3049.659	28.2011	771.6269	21.3048	3000.195	30.2607
876.045	4.712	3124.367	24.5532	864.5634	11.1667	3064.382	32.9571
1105.55	108.902	3155.001	16.7675	1113.621	127.531	3144.824	8.5787
1153.89	289.927	3808.569	89.8579	1132.077	72.7535	3825.338	49.6949
1171.23	0.4494			1163.522	0.8332		
Isomer 2a				Isomer 2b			
							
Energy (hartree): -303.904082				Energy (hartree): -303.899638			
Relative energy (kJ mol ⁻¹): 3.6				Relative energy (kJ mol ⁻¹): 6.4			
Adiabatic IE (eV): 10.52 ± 0.05 (2c⁺)				Adiabatic IE (eV): 10.39 ± 0.05 (2a⁺)			
	x	y	z		z	y	z
O	-0.135204	0.062694	0.046339	O	-0.120561	0.025478	0.010743
C	-0.011537	-0.195611	1.420541	C	0.035145	-0.037213	1.409104
C	1.441934	-0.271415	1.834894	C	1.468811	0.041017	1.908846
O	2.358787	-0.126164	1.064228	O	1.791853	0.323818	3.030907
O	1.596291	-0.516953	3.147199	O	2.354158	-0.307357	0.943163
H	-0.493195	0.589828	2.017191	H	-0.509571	0.799936	1.846596
H	-0.490479	-1.145582	1.691033	H	-0.386876	-0.959636	1.839064
H	0.766457	0.127165	-0.299123	H	0.526269	-0.567014	-0.386330
H	2.548556	-0.549175	3.324306	H	3.236923	-0.270260	1.340652
Freq.	Int.	Freq.	Int.	Freq.	Int.	Freq.	Int.
59.7354	17.9628	1245.733	0.311	79.4328	2.2352	1239.868	39.4087
283.132	8.9694	1296.44	30.109	251.5929	43.6955	1341.169	23.5211
297.43	76.5143	1358.126	118.367	322.9643	101.929	1365.727	25.1327
472.793	25.1552	1469.482	19.4244	478.9678	11.2837	1424.603	73.8172

Table A1
(Continued)

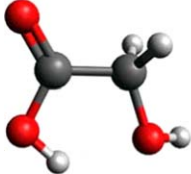
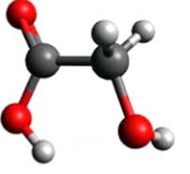
504.274	7.0426	1495.22	5.4921	525.0565	23.1342	1484.997	6.0789
652.905	18.0222	1820.78	288.352	606.9203	84.4244	1843.421	281.07
659.222	131.129	3004.806	31.03	684.2626	94.3229	2969.163	37.6212
859.158	40.5843	3026.37	22.6993	835.0274	19.9483	3109.67	8.7178
1041.45	1.8337	3740.873	73.9708	1011.717	16.6857	3761.468	68.0865
1113.12	223.218	3756.261	65.3313	1095.922	97.5613	3828.488	43.3417
1180.85	148.379			1162.954	223.979		
Isomer 2c				Isomer 2d			
							
Energy (hartree): -303.898547				Energy (hartree): -303.898053			
Relative energy (kJ mol ⁻¹): 7.1				Relative energy (kJ mol ⁻¹): 7.4			
Adiabatic IE (eV): 10.37 ± 0.05 (2b ⁺)				Adiabatic IE (eV): 10.36 ± 0.05 (2b ⁺)			
	x	y	z		z	y	z
O	0.074565	-0.018970	0.007020	O	0.186184	-0.238282	-0.046894
C	0.049619	0.051592	1.432799	C	0.134363	-0.023218	1.366070
C	1.472498	-0.101919	1.972401	C	1.516456	-0.136287	2.019307
O	1.731183	0.032080	3.135082	O	1.672703	-0.136678	3.207579
O	2.388164	-0.411421	1.042239	O	2.529940	-0.207250	1.139641
H	-0.340870	1.011675	1.783557	H	-0.228259	0.993566	1.533946
H	-0.551103	-0.749391	1.876022	H	-0.545976	-0.709694	1.874711
H	-0.758824	-0.369462	-0.317299	H	-0.046292	-1.154025	-0.227735
H	1.925269	-0.449926	0.186761	H	2.130294	-0.178442	0.251957
Freq.	Int.	Freq.	Int.	Freq.	Int.	Freq.	Int.
107.394	2.6657	1229.739	5.7658	96.9857	20.8979	1217.294	7.5131
146.264	119.184	1281.301	26.1568	296.4482	110.006	1360.4	14.052
321.488	16.661	1396.316	332.516	314.1198	13.8974	1369.152	10.6646
509.868	4.2388	1409.316	82.5889	494.8492	4.4983	1389.771	409.133
562.754	23.0064	1491.025	9.926	551.0609	12.9548	1475.93	9.469
632.343	15.2985	1870.753	293.433	647.0612	11.6222	1870.307	284.252
702.985	89.7886	3031.038	18.6392	751.4364	87.8042	3058.493	13.172
854.231	8.3855	3074.821	16.4348	859.6138	23.6371	3106.429	8.8959
1012.71	6.608	3662.622	154.135	980.7477	24.6721	3651.758	141.658
1066.73	59.3282	3864.251	51.7637	1052.429	61.0229	3841.695	51.0738
1164.95	104.24			1175.114	55.9433		
Isomer 2e				Isomer 2f			

Table A1
(Continued)

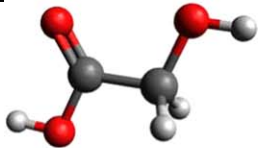
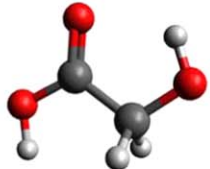
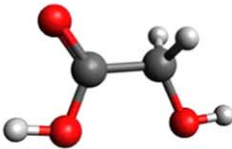
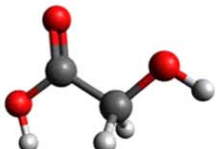
							
Energy (hartree): -303.896807 Relative energy (kJ mol ⁻¹): 8.2 Adiabatic IE (eV): 10.33 ± 0.05 (2c⁺)				Energy (hartree): -303.896596 Relative energy (kJ mol ⁻¹): 8.3 Adiabatic IE (eV): 10.32 ± 0.05 (2b⁺)			
	x	y	z		z	y	z
O	-0.009855	0.358813	0.052527	O	-0.120043	0.019454	0.057621
C	0.043603	-0.128862	1.371597	C	-0.002734	-0.228382	1.429819
C	1.487470	-0.145171	1.832584	C	1.457224	-0.208772	1.867369
O	2.446461	0.194548	1.201346	O	2.349401	-0.001651	1.091431
O	1.552474	-0.614262	3.105592	O	1.704501	-0.435848	3.174320
H	-0.516573	0.494028	2.083514	H	-0.548067	0.528570	2.013257
H	-0.338141	-1.155465	1.466414	H	-0.427672	-1.209727	1.688851
H	-0.930912	0.362269	-0.221945	H	0.785926	0.143074	-0.264719
H	2.488172	-0.606541	3.354981	H	0.880059	-0.583151	3.655049
Freq.	Int.	Freq.	Int.	Freq.	Int.	Freq.	Int.
75.5638	17.8426	1245.78	23.7374	89.8861	7.3354	1253.673	1.3628
201.391	116.411	1255.182	0.2338	289.0041	31.4524	1291.432	91.3503
266.758	2.1102	1331.904	9.6136	343.9085	52.5449	1321.278	392.127
473.548	7.8453	1461.403	23.2514	440.977	151.754	1459.072	18.7768
510.063	20.7643	1501.322	6.2708	471.5927	0.6296	1500.275	5.9725
630.81	46.833	1864.763	292.208	569.1226	0.2746	1853.445	233.316
653.651	114.596	2981.722	35.8018	665.9093	13.4859	2973.571	42.5326
845.484	2.0032	3008.901	30.8733	863.4339	1.2906	2992.196	33.2411
1038.02	0.0267	3765.721	62.1427	1037.536	0.6537	3712.475	79.4642
1105.1	341.187	3849.7	40.5863	1122.32	159.46	3794.532	52.2221
1153.41	121.963			1176.523	5.2912		
<p style="text-align: center;">Isomer 2g</p> 				<p style="text-align: center;">Isomer 2h</p> 			
Energy (hartree): -303.896064 Relative energy (kJ mol ⁻¹): 8.6 Adiabatic IE (eV): 10.29 ± 0.05 (2a⁺)				Energy (hartree): -303.887772 Relative energy (kJ mol ⁻¹): 13.8 Adiabatic IE (eV): 10.08 ± 0.05 (2b⁺)			
Atom	x	y	z	Atom	z	y	z
O	-0.028019	-0.043893	-0.026388	O	0.003466	0.323511	0.071252
C	0.038744	0.006551	1.382017	C	0.056216	-0.128544	1.399596
C	1.469731	-0.019008	1.884509	C	1.499907	-0.059676	1.891771
O	1.739514	0.016449	3.058568	O	2.429210	0.317235	1.249894

Table A1
(Continued)

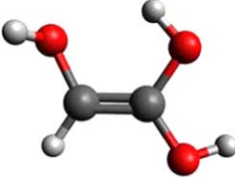
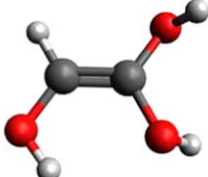
O	2.390191	-0.083907	0.909413	O	1.660385	-0.479908	3.179895
H	-0.406984	0.921432	1.796142	H	-0.555654	0.485857	2.079845
H	-0.461676	-0.845714	1.862023	H	-0.280384	-1.172724	1.504475
H	-0.955581	-0.024611	-0.278205	H	-0.909958	0.274538	-0.224655
H	3.251320	-0.093961	1.354664	H	0.816494	-0.752152	3.560925
Freq.	Int.	Freq.	Int.	Freq.	Int.	Freq.	Int.
33.0636	22.174	1246.88	54.3832	59.5913	20.919	1240.088	138.275
206.053	118.132	1263.568	0.1495	203.2675	91.2995	1263.391	0.0092
273.309	7.0219	1384.027	45.0925	269.0942	1.2848	1288.093	250.665
505.59	3.2378	1453.634	18.3133	401.8546	128.419	1446.061	29.7536
525.122	14.1705	1497.803	6.0881	472.5115	4.9549	1506.637	3.2266
596.305	57.986	1826.13	291.041	573.0167	0.0741	1897.292	246.701
700.411	126.256	2989.589	32.3542	642.4601	14.2813	2948.826	48.217
841.51	1.1928	3017.755	27.3287	846.4811	37.1352	2973.504	42.6147
1033.3	0.0047	3750.945	57.9407	1034.009	0.1083	3795.904	33.6783
1107.27	60.3362	3844.217	33.2847	1106.218	161.59	3845.138	40.2455
1176.4	346.267			1142.226	4.0733		
<p>Isomer 3a</p> 				<p>Isomer 3b</p> 			
Energy (hartree): -303.861573				Energy (hartree): -303.859288			
Relative energy (kJ mol ⁻¹): 30.3				Relative energy (kJ mol ⁻¹): 31.7			
Adiabatic IE (eV): 7.80 ± 0.05 (3a⁺)				Adiabatic IE (eV): 8.01 ± 0.05 (3e⁺)			
	x	y	z		z	y	z
C	-0.124688	0.009585	0.046574	C	-0.032600	0.020407	0.010492
C	0.034421	0.142883	1.366673	C	-0.006242	0.005519	1.341130
O	1.231020	0.106798	1.987854	O	1.147470	-0.072722	2.072574
O	-1.004248	0.328057	2.220484	O	-1.186913	0.045736	2.059458
O	-1.434370	0.117468	-0.444525	O	-1.177798	-0.035087	-0.733779
H	0.698866	-0.071265	-0.648236	H	0.872850	0.075843	-0.574751
H	1.105259	0.453185	2.879026	H	1.197485	0.702398	2.647467
H	-1.792254	0.416406	1.662496	H	-1.183491	-0.691746	2.683917
H	-1.678069	-0.719420	-0.854483	H	-1.918450	-0.050349	-0.113757
Freq.	Int.	Freq.	Int.	Freq.	Int.	Freq.	Int.
175.925	106.0763	1210.6615	197.2192	241.9191	1.0906	1198.8514	46.6857
258.362	2.6399	1228.0067	6.2829	277.539	53.5737	1266.1373	194.5114
287.158	102.6102	1235.7533	95.7266	316.0408	59.605	1274.0426	16.2169
361.227	90.1714	1379.5271	73.6564	405.5253	59.7567	1313.2454	90.67
480.596	18.8427	1420.9921	139.1299	490.2135	98.1888	1404.2203	47.6596

Table A1
(Continued)

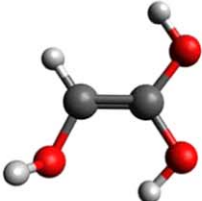
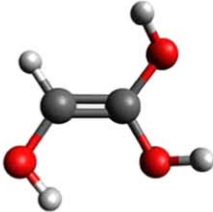
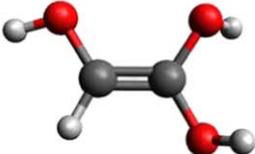
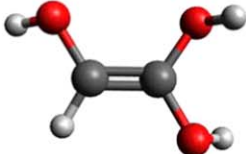
538.92	117.4732	1799.0532	167.9503	511.7038	60.8522	1804.6785	14.1064
634.24	10.225	3213.5206	11.2695	526.1039	122.3959	3238.5614	6.5351
645.486	22.1848	3736.6992	71.3232	636.7356	16.4627	3750.4731	35.2422
697.337	30.7378	3791.5318	37.0663	845.8778	34.7843	3761.8132	30.2355
943.635	42.2845	3818.7033	97.1713	898.097	45.1779	3784.7406	41.1639
1089.88	183.7372			1130.0047	301.6604		
Isomer 3c				Isomer 3d			
							
Energy (hartree): -303.858678				Energy (hartree): -303.858221			
Relative energy (kJ mol ⁻¹): 32.1				Relative energy (kJ mol ⁻¹): 32.4			
Adiabatic IE (eV): 7.91 ± 0.05 (3c⁺)				Adiabatic IE (eV): 7.87 ± 0.05 (3b⁺)			
	x	y	z		z	y	z
C	-0.118672	-0.027449	0.073089	C	-0.042383	0.062649	-0.029898
C	0.007711	-0.051406	1.408358	C	-0.019880	-0.009084	1.301358
O	1.158341	0.019088	2.110756	O	1.085687	0.007698	2.112560
O	-1.040693	-0.164926	2.241804	O	-1.181836	-0.061787	2.015214
O	-1.408102	-0.209169	-0.450303	O	-1.191611	-0.015709	-0.783157
H	0.718457	-0.004154	-0.614097	H	0.849963	0.210858	-0.621162
H	1.889606	0.130002	1.494079	H	1.854768	-0.258495	1.598344
H	-1.810034	-0.297616	1.667523	H	-1.028919	-0.607584	2.796250
H	-1.677322	0.605631	-0.888196	H	-1.930125	-0.112242	-0.169607
Freq.	Int.	Freq.	Int.	Freq.	Int.	Freq.	Int.
240.272	32.3369	1195.3108	388.6334	223.5375	46.9845	1184.7504	240.2813
260.955	8.5736	1237.9071	36.1282	239.9946	43.3236	1223.2719	44.6007
322.49	45.6951	1244.2454	28.2159	280.3594	84.2308	1281.2694	96.0082
371.777	102.6455	1384.9527	93.7019	307.8238	37.5599	1370.0058	132.7393
491.345	10.9559	1466.7719	34.1219	398.9255	162.331	1431.0186	79.0192
560.594	211.0981	1754.4256	229.9818	482.6971	24.1085	1802.2799	38.0847
637.73	14.4394	3176.7357	21.8946	543.3962	6.4811	3218.2786	12.8983
654.573	31.366	3744.1816	74.7665	633.7592	13.4081	3794.8172	61.0806
665.817	14.8905	3787.465	35.0125	759.5282	58.0234	3801.6434	45.3582
957.198	33.2515	3840.3225	57.2751	918.6959	42.2029	3841.5438	50.3203
1098.47	81.8148			1115.6406	181.8596		
Isomer 3e				Isomer 3f			
							

Table A1
(Continued)

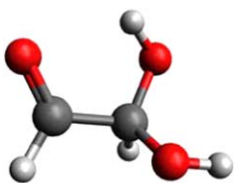
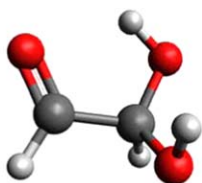
Energy (hartree): -303.854184 Relative energy (kJ mol ⁻¹): 34.9 Adiabatic IE (eV): 7.87 ± 0.05 (3d⁺)				Energy (hartree): -303.85407 Relative energy (kJ mol ⁻¹): 35.0 Adiabatic IE (eV): 7.83 ± 0.05 (3d⁺)			
	x	y	z		x	y	z
C	-0.086466	0.107391	0.027022	C	-0.066717	0.122613	0.014836
C	-0.049304	0.035402	1.355957	C	-0.032403	0.050013	1.344124
O	1.149525	0.026202	2.026931	O	1.162882	-0.088707	2.005436
O	-1.170048	-0.038491	2.133883	O	-1.147466	0.073974	2.131945
O	-1.271964	0.220126	-0.661072	O	-1.245097	0.00722	-0.686265
H	0.838449	0.042164	-0.532478	H	0.863799	0.200609	-0.53589
H	1.159537	-0.746346	2.607175	H	1.182438	0.564719	2.716557
H	-1.101377	0.637862	2.820145	H	-1.134509	-0.709062	2.697633
H	-1.072687	0.499387	-1.55766	H	-1.187264	0.562318	-1.468474
Freq.	Int.	Freq.	Int.	Freq.	Int.	Freq.	Int.
68.9526	95.2797	1194.3116	178.6294	156.5027	156.6634	1194.6215	195.8727
234.716	77.7725	1241.029	130.5795	224.8199	143.6995	1240.6203	108.2751
263.041	98.0148	1276.7471	70.0816	264.1408	28.3938	1276.5248	32.927
328.708	51.9332	1316.0235	56.7153	318.7038	12.7878	1306.9407	60.2658
420.876	47.2362	1400.3975	35.8389	428.3443	45.7334	1395.9795	41.8918
522.785	91.9348	1827.2281	21.1537	528.4223	103.4216	1820.0969	26.8672
527.238	24.6363	3189.2498	12.3655	538.3421	29.7425	3176.1769	15.5471
629.535	35.9806	3755.6229	31.027	632.5144	33.3079	3762.4516	39.705
804.077	30.495	3767.1578	29.3352	809.9783	29.8798	3768.1865	27.6011
904.387	49.9009	3866.557	76.3926	908.6261	54.0406	3846.3446	65.9285
1136.69	241.8559			1137.2756	260.6949		
Isomer 4a				Isomer 4b			
							
Energy (hartree): -303.874532 Relative energy (kJ mol ⁻¹): 22.2 Adiabatic IE (eV): 9.81 ± 0.05 (4b⁺)				Energy (hartree): -303.873644 Relative energy (kJ mol ⁻¹): 22.7 Adiabatic IE (eV): 9.11 ± 0.05 (4a⁺)			
	x	y	z		x	y	z
O	-0.276147	0.165001	0.208299	O	0.184026	-0.165564	-0.022461
C	-0.010149	0.173815	1.570000	C	-0.008824	0.149510	1.346879
C	1.497457	0.147274	1.840359	C	1.359587	0.042663	2.031759
O	2.292433	0.034732	0.944519	O	1.560365	-0.749459	2.919209
O	-0.489849	-0.965599	2.259926	O	-0.921345	-0.685479	1.975376
H	0.491253	-0.238073	-0.225728	H	0.268464	-1.125527	-0.081131
H	-0.452159	1.090977	1.983863	H	-0.365108	1.184609	1.351944

Table A1
(Continued)

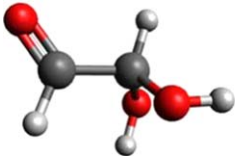
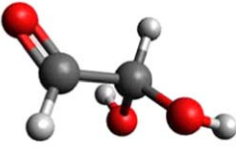
H	1.800907	0.196650	2.902279	H	2.160380	0.680481	1.614938
H	-1.440440	-1.012662	2.111395	H	-0.414551	-1.207561	2.619080
Freq.	Int.	Freq.	Int.	Freq.	Int.	Freq.	Int.
133.033	3.3303	1219.229	59.5329	107.0321	2.5912	1272.557	54.1653
249.927	46.351	1310.931	28.0843	298.3165	57.0818	1300.368	18.2342
291.535	110.789	1376.113	7.481	317.0539	73.5733	1372.569	11.7686
361.022	2.1978	1401.901	26.407	378.3502	3.1978	1423.008	87.9013
436.776	95.0251	1478.115	60.9701	460.0644	109.008	1452.054	57.4715
551.523	36.3271	1822.624	123.414	564.1331	14.8034	1803.147	126.306
733.564	13.806	2955.346	70.7111	742.0343	10.172	2960.142	70.461
839.201	42.7733	2998.054	61.7949	839.922	30.1307	3048.714	37.8912
977.874	101.366	3723.049	59.6657	1016.18	33.7083	3678.362	78.4473
1069.15	71.7744	3824.169	46.6862	1034.753	148.023	3795.666	34.9605
1134.33	133.73			1125.793	88.0921		
Isomer 4c 				Isomer 4d 			
Energy (hartree): -303.871152				Energy (hartree): -303.86952			
Relative energy (kJ mol ⁻¹): 24.3				Relative energy (kJ mol ⁻¹): 25.3			
Adiabatic IE (eV): 9.04 ± 0.05 (4a⁺)				Adiabatic IE (eV): 9.00 ± 0.05 (4a⁺)			
	x	y	z		x	y	z
O	0.339029	0.357060	0.093039	O	0.317691	0.443232	0.081159
C	0.115385	0.094565	1.453587	C	0.117011	0.187178	1.429867
C	1.501732	-0.004776	2.088717	C	1.494002	-0.005152	2.064301
O	1.842995	0.609036	3.061239	O	1.766554	0.380467	3.170017
O	-0.592066	-1.108022	1.657419	O	-0.594672	-1.039905	1.551206
H	-0.514658	0.502565	-0.330311	H	-0.539660	0.410131	-0.358510
H	-0.462763	0.872445	1.958602	H	-0.415402	0.996113	1.952436
H	2.170752	-0.734749	1.577991	H	2.195147	-0.589128	1.433589
H	-0.116752	-1.808118	1.191025	H	-0.985550	-1.079746	2.431530
Freq.	Int.	Freq.	Int.	Freq.	Int.	Freq.	Int.
94.3121	5.0637	1233.456	57.6115	81.5544	14.1927	1240.954	78.6101
302.831	71.5392	1276.302	8.4163	278.8761	76.2429	1269.27	73.0872
316.316	9.2765	1383.564	6.3464	299.3789	32.7926	1363.172	16.5848
366.758	28.2554	1429.668	62.0482	315.2287	129.003	1402.508	22.6735
404.765	115.698	1433.82	4.2935	380.7309	37.9995	1448.415	22.1602
477.862	79.9149	1841.047	146.093	463.7327	41.16	1827.901	135.313
618.609	32.7947	2861.784	106.18	611.0113	3.9421	2917.971	76.9234
972.7	65.4485	3077.321	32.0223	967.2526	33.7946	2978.728	76.6686
1001.63	30.9774	3781.119	27.3807	1018.533	45.7904	3811.585	47.9792

Table A1
(Continued)

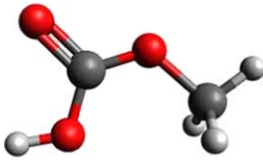
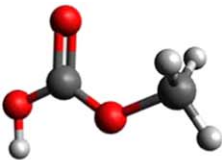
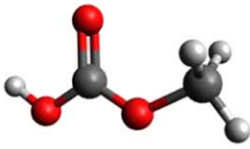
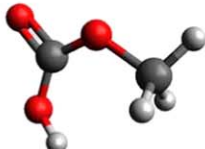
1048.79	110.293	3813.539	47.2274	1045.873	3.6508	3817.807	41.4095
1086.16	144.536			1096.061	189.745		
<p style="text-align: center;">Isomer 1a⁺</p>  <p>Energy (hartree): -303.508385 Relative energy (kJ mol⁻¹): 41.8</p>				<p style="text-align: center;">Isomer 1b⁺</p>  <p>Energy (hartree): -303.508115 Relative energy (kJ mol⁻¹): 41.9</p>			
	x	y	z		x	y	z
C	-0.023832	0.040309	-0.086546	C	-0.002099	0.144379	-0.117483
O	0.246461	-0.150492	1.382535	O	0.407084	-0.567618	1.148530
C	1.401972	-0.064074	1.862519	C	1.475824	-0.320098	1.792561
O	2.448098	0.193059	1.147148	O	1.800769	-0.936731	2.862644
O	1.553774	-0.240713	3.134014	O	2.281897	0.589433	1.364927
H	-1.096814	-0.100346	-0.151214	H	-0.945515	-0.329534	-0.363284
H	0.278368	1.050040	-0.352195	H	-0.121458	1.199669	0.115541
H	0.527556	-0.723679	-0.628525	H	0.760258	-0.044763	-0.869296
H	3.294512	0.235362	1.633528	H	1.147915	-1.611932	3.131344
Freq.	Int.	Freq.	Int.	Freq.	Int.	Freq.	Int.
52.2401	0.666	1189.51	15.4027	110.4876	0.1062	1198.842	11.432
115.207	20.521	1429.103	124.791	141.8453	13.67	1415.381	221.321
229.959	4.1786	1461.185	22.8531	216.3366	14.7816	1467.517	14.1295
427.292	24.2889	1476.54	22.6702	459.2257	164.963	1483.056	23.7961
449.883	173.366	1478.961	120.568	469.1113	0.2962	1516.405	152.153
585.775	16.7326	1688.517	450.662	497.8033	7.7803	1642.541	359.903
748.762	17.8898	3087.885	0.3555	740.9258	31.1419	3085.521	0.0738
807.574	62.537	3201.345	0.2384	803.5459	114.504	3197.724	0.6091
1053.7	33.2062	3223.753	3.9693	1053.568	72.0921	3223.701	4.3566
1136.88	149.443	3667.899	330.196	1136.691	71.3386	3674.013	330.883
1137.94	0.6381			1152.58	0.7676		
<p style="text-align: center;">Isomer 1c⁺</p>  <p>Energy (hartree): -303.507853 Relative energy (kJ mol⁻¹): 42.1</p>				<p style="text-align: center;">Isomer 1d⁺</p>  <p>Energy (hartree): -303.499847 Relative energy (kJ mol⁻¹): 47.1</p>			
	x	y	z		x	y	z
C	-0.032596	0.146901	-0.079215	C	-0.061358	0.011420	-0.087908
O	0.378521	-0.491980	1.217307	O	0.228899	-0.001948	1.376950
C	1.499184	-0.311637	1.777249	C	1.400181	-0.020682	1.855701

Table A1
(Continued)

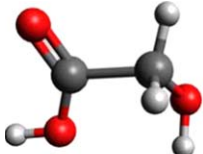
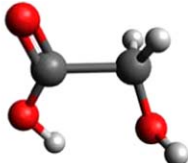
O	1.717384	-0.924385	2.888886	O	2.531294	0.174764	1.279992
O	2.390309	0.449922	1.265862	O	1.473780	-0.294077	3.121048
H	-1.033828	-0.240970	-0.228588	H	-1.121096	-0.215103	-0.136011
H	-0.029436	1.225450	0.059174	H	0.140848	1.015653	-0.458495
H	0.653926	-0.187051	-0.853548	H	0.531000	-0.762891	-0.573229
H	2.591875	-0.761331	3.291279	H	2.495561	0.561599	0.387545
Freq.	Int.	Freq.	Int.	Freq.	Int.	Freq.	Int.
99.5353	1.1704	1197.174	48.2894	76.3647	2.323	1189.408	13.067
128.172	3.0977	1415.393	66.0619	101.5396	0.1294	1438.015	102.895
210.156	11.4763	1460.079	85.328	218.3614	6.5802	1461.994	17.7989
417.097	16.4741	1476.728	102.533	345.4094	125.31	1490.453	27.4938
427.137	178.553	1484.108	23.9578	463.5924	30.1277	1573.172	159.802
508.457	36.8898	1532.051	211.681	580.186	28.8021	1628.425	433.468
740.941	25.9715	3084.778	0.2135	745.5641	29.0943	3066.925	1.9875
813.992	24.0412	3195.942	0.2969	823.5254	48.1936	3174.648	0.7428
1064.95	5.8496	3221.808	5.2217	1060.511	27.933	3209.207	6.1819
1147.45	209.041	3681.815	368.894	1101.314	201.334	3715.834	236.715
1153.92	1.3961			1138.389	3.0651		
 <p>Isomer 2a⁺</p>				 <p>Isomer 2b⁺</p>			
Energy (hartree): -303.517851				Energy (hartree): -303.517469			
Relative energy (kJ mol ⁻¹): 35.8				Relative energy (kJ mol ⁻¹): 36.1			
	x	y	z		x	y	z
O	-0.033238	0.188870	0.064482	O	-0.131431	-0.969353	0.776787
C	-0.022022	-0.046513	1.389152	C	0.051666	0.217756	1.395641
C	1.563139	0.085665	1.930757	C	1.498078	0.074692	2.298096
O	1.728928	0.586347	2.992605	O	2.014938	1.116949	2.536570
O	2.372195	-0.433508	1.057212	O	1.825802	-1.121410	2.631539
H	-0.590335	0.709500	1.923093	H	0.157949	1.098680	0.765743
H	-0.233222	-1.081467	1.694847	H	-0.646407	0.338884	2.231288
H	0.305592	-0.560851	-0.457595	H	0.082198	-0.940575	-0.171525
H	3.305115	-0.399276	1.348191	H	1.225802	-1.792054	2.248859
Freq.	Int.	Freq.	Int.	Freq.	Int.	Freq.	Int.
82.9146	5.5549	1205.497	54.0792	124.6842	13.1938	1212.73	85.0006
253.357	0.0768	1258.037	80.9312	255.6829	15.1358	1248.756	117.175
364.2	10.0554	1333.808	4.6101	341.2006	5.9337	1313.251	118.017
420.48	46.8264	1376.756	65.6124	422.4736	37.572	1366.883	66.7234
537.181	46.6227	1484.849	4.8118	537.4653	18.5186	1488.584	2.2249
573.3	53.1897	1816.597	185.132	579.93	104.022	1806.425	151.071

Table A1
(Continued)

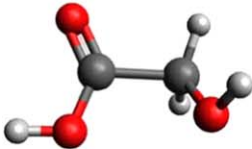
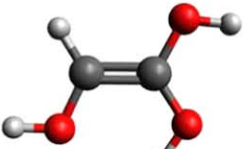
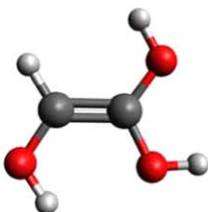
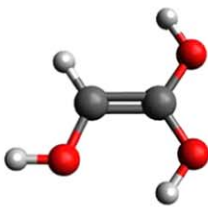
578.677	124.271	2999.29	22.344	624.9155	95.4567	3041.247	28.6371
683.767	69.3198	3189.838	9.1102	666.9995	88.612	3172.387	9.1679
958.988	36.855	3654.551	293.012	940.5475	18.8194	3633.305	114.681
1116.03	70.9044	3692.662	315.249	1142.912	140.416	3716.953	340.894
1152.59	97.2686			1152.914	40.929		
Isomer 2c⁺ 				Isomer 3a⁺ 			
Energy (hartree): -303.517358 Relative energy (kJ mol ⁻¹): 36.1				Energy (hartree): -303.574928 Relative energy (kJ mol ⁻¹): 0.0			
	x	y	z		x	y	z
O	-0.010360	0.797952	0.728529	C	-0.191671	-0.105105	0.076913
C	0.055545	-0.447406	1.235961	C	-0.010502	0.196837	1.446888
C	1.520130	-0.600316	2.044993	O	1.199980	0.260352	1.901844
O	2.059135	-1.653529	1.928117	O	-0.991963	0.413407	2.271428
O	1.803403	0.478304	2.697594	O	-1.444660	-0.155867	-0.327398
H	-0.606233	-0.541017	2.108485	H	0.649401	-0.280075	-0.582425
H	-0.009409	-1.274683	0.532193	H	1.231923	0.472785	2.852236
H	0.134431	0.821770	-0.233874	H	-1.865802	0.345838	1.846357
H	2.634970	0.393711	3.204612	H	-1.540766	-0.364475	-1.269981
Freq.	Int.	Freq.	Int.	Freq.	Int.	Freq.	Int.
55.2472	9.037	1190.941	123.422	228.5534	22.9421	1199.0654	183.3925
257.286	2.8196	1262.666	41.2252	255.5948	4.3581	1220.827	179.928
352.148	4.1907	1341.135	12.0046	470.9252	229.6091	1309.1197	172.0241
405.459	77.8184	1361.727	27.6557	496.7148	19.4538	1455.905	147.3468
534.679	97.374	1481.462	11.28	536.8579	158.9761	1582.5748	220.1343
574.357	62.1122	1812.08	217.703	573.3355	53.2338	1688.774	88.3828
610.886	123.952	3005.352	37.7002	642.7024	27.1979	3217.852	28.8833
691.449	83.1456	3165.468	7.4338	662.4817	27.2561	3697.2967	242.9257
939.014	8.904	3657.601	312.157	765.7392	8.6633	3704.2843	313.5194
1127.87	53.5235	3704.554	347.718	946.9384	10.9357	3757.7348	321.0316
1158.05	118.794			1144.6158	125.6715		
Isomer 3b⁺ 				Isomer 3c⁺ 			
Energy (hartree): -303.569004				Energy (hartree): -303.567991			

Table A1
(Continued)

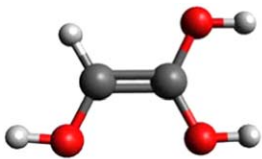
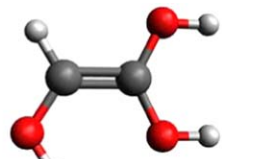
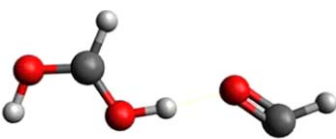
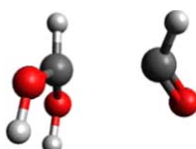
Relative energy (kJ mol ⁻¹): 3.7				Relative energy (kJ mol ⁻¹): 4.4					
	x	y	z		x	y	z		
	C	-0.047069	0.045773	-0.061333		C	-0.181374	0.097011	0.086408
	C	-0.016336	-0.131702	1.339726		C	0.003290	-0.078661	1.484190
	O	1.057570	-0.160098	2.077262		O	1.160470	-0.089486	2.068601
	O	-1.160792	-0.279690	1.946180		O	-0.988888	-0.244446	2.296134
	O	-1.157757	0.064899	-0.744252		O	-1.436224	0.078261	-0.318811
	H	0.855998	0.176089	-0.645401		H	0.640368	0.237012	-0.606317
	H	1.890994	-0.046788	1.591911		H	1.912725	0.034007	1.469492
	H	-1.074227	-0.397657	2.909062		H	-1.848107	-0.233285	1.838876
	H	-1.952717	-0.054523	-0.193255		H	-1.542968	0.199586	-1.275560
Freq.	Int.	Freq.	Int.	Freq.	Int.	Freq.	Int.		
219.109	15.1585	1176.6685	248.3017	212.6199	21.6566	1171.6436	81.1254		
260.077	10.4489	1241.6455	97.1946	269.5588	4.7017	1230.6562	209.1574		
454.328	240.9049	1381.3796	31.7948	437.0278	2.4308	1306.9225	223.3219		
488.243	11.569	1429.4766	368.3425	481.1172	146.6841	1445.8228	209.43		
509.726	25.7584	1572.6786	158.7048	510.4399	6.368	1606.0964	135.3109		
552.395	92.8752	1679.5381	42.7401	596.6809	265.3712	1648.3202	109.3453		
639.514	45.349	3214.9266	24.7059	655.6514	10.2697	3200.9208	20.5728		
657.322	13.4771	3687.0034	175.948	660.8977	30.0173	3708.7454	201.1901		
850.327	108.2267	3709.2922	359.2348	729.5978	6.6398	3754.4753	381.6246		
956.976	15.4312	3743.9636	206.1643	954.9146	32.4003	3767.3992	189.8336		
1142.85	123.2183			1164.1246	152.6885				
Isomer 3d ⁺				Isomer 3e ⁺					
									
Energy (hartree): -303.566069				Energy (hartree): -303.564926					
Relative energy (kJ mol ⁻¹): 5.6				Relative energy (kJ mol ⁻¹): 6.3					
	x	y	z		x	y	z		
	C	-0.068460	0.113759	-0.052778		C	-0.051871	0.064836	-0.065849
	C	-0.042312	0.030994	1.357436		C	-0.014558	0.030186	1.343834
	O	1.112046	-0.269172	1.893126		O	1.143063	0.201761	1.919579
	O	-1.144338	0.254099	2.014081		O	-1.154733	-0.173052	1.963028
	O	-1.205596	0.412166	-0.624275		O	-1.146807	-0.092915	-0.752659
	H	0.838317	-0.068749	-0.617530		H	0.852769	0.228048	-0.637130
	H	1.130835	-0.327068	2.861163		H	1.151892	0.174067	2.889397
	H	-1.086020	0.188688	2.980183		H	-1.131846	-0.196132	2.932459
	H	-1.138808	0.448981	-1.591504		H	-1.935598	-0.236799	-0.199909
Freq.	Int.	Freq.	Int.	Freq.	Int.	Freq.	Int.		

Table A1
(Continued)

188.34	4.162	1145.5899	196.1778	174.0694	5.152	1133.6741	296.4771
268.937	9.9265	1228.3802	102.2622	260.7893	1.1107	1231.4993	79.1672
310.997	1.582	1325.3064	154.801	283.1133	2.7076	1378.5704	11.4878
460.382	390.9486	1457.7461	102.7464	421.8056	284.2318	1443.0442	186.7641
501.46	60.2181	1552.4052	261.2907	493.6486	10.6329	1535.0281	277.6776
504.153	7.5544	1704.0172	26.0379	525.3812	70.3858	1692.5892	8.95
635.311	21.3416	3207.1691	24.0128	646.5741	27.3316	3231.9348	32.7748
649.515	29.7452	3748.7002	103.5073	648.4171	37.3171	3696.003	166.9783
812.798	6.3338	3752.7533	642.5939	880.0549	83.0764	3747.7425	66.0099
942.339	28.0681	3764.5706	143.0557	945.4417	44.4453	3762.0011	501.8336
1126.29	265.3815			1116.5503	207.043		
Isomer 4a⁺ 				Isomer 4b⁺ 			
Energy (hartree): -303.538790				Energy (hartree): -303.514137			
Relative energy (kJ mol ⁻¹): 22.7				Relative energy (kJ mol ⁻¹): 38.1			
	x	y	z		x	y	z
O	-1.779174	0.379596	-0.056067	O	-0.259766	0.351665	0.194924
C	-0.772121	0.439056	0.719554	C	-0.315762	0.301843	1.493468
C	2.640780	-0.687124	3.169531	C	1.860927	0.152511	2.026402
O	1.813859	-0.027750	2.626958	O	2.560602	-0.112087	1.147305
O	-0.140329	-0.593912	1.061016	O	-0.813969	-0.681206	2.196953
H	-1.994724	-0.530508	-0.343788	H	-0.334517	-0.497110	-0.272127
H	-0.503892	1.439327	1.059642	H	-0.362836	1.270202	1.980111
H	3.441005	-0.291542	3.832547	H	2.027815	0.323033	3.108611
H	0.649719	-0.423955	1.686202	H	-0.949189	-1.516736	1.719264
Freq.	Int.	Freq.	Int.	Freq.	Int.	Freq.	Int.
47.0801	2.5731	1205.504	222.3518	38.2502	19.6485	1115.191	222.5183
69.9528	1.8722	1314.919	24.2274	81.5612	21.9584	1124.773	135.9796
125.263	0.0241	1388.856	100.9596	148.7055	9.4184	1360.296	48.6775
152.241	17.5384	1497.127	188.1092	265.9947	6.795	1399.783	15.0389
277.198	76.859	1707.986	538.8901	382.4069	13.0721	1530.034	288.5597
323.453	32.3215	1873.01	239.9127	434.7358	5.8313	1994.763	189.1363
637.835	3.2855	2794.154	2840.7	564.0838	190.6209	2914.182	6.8584
771.401	214.0741	2867.813	308.0655	597.252	233.8281	3200.926	19.4983
1029.76	113.603	3170.776	2.3707	681.1876	64.8398	3721.785	67.2697
1108.99	1.7137	3649.608	210.2824	960.9178	161.6192	3731.732	338.0467
1127.16	88.9501			1058.556	21.3956		

ORCID iDs

Joshua H. Marks  <https://orcid.org/0000-0003-0492-2494>
 Jia Wang  <https://orcid.org/0000-0002-3795-8699>
 Mikhail M. Evseev  <https://orcid.org/0000-0003-2687-2192>
 Oleg V. Kuznetsov  <https://orcid.org/0000-0003-2387-9591>
 Ralf I. Kaiser  <https://orcid.org/0000-0002-7233-7206>

References

- Abplanalp, M. J., Borsuk, A., Jones, B. M., & Kaiser, R. I. 2015, *ApJ*, **814**, 45
 Abplanalp, M. J., Förstel, M., & Kaiser, R. I. 2016a, *CPL*, **644**, 79
 Abplanalp, M. J., Gozem, S., Krylov, A. I., et al. 2016b, *PNAS*, **113**, 7727
 Abplanalp, M. J., Góbi, S., & Kaiser, R. I. 2019, *PCCP*, **21**, 5378
 Agarwal, V. K., Schutte, W., Greenberg, J. M., et al. 1985, *OLEB*, **16**, 21
 Bennett, C. J., Chen, S. H., Sun, B. J., Chang, A. H. H., & Kaiser, R. I. 2007, *ApJ*, **660**, 1588
 Bennett, C. J., Jamieson, C. S., Osamura, Y., & Kaiser, R. I. 2005a, *ApJ*, **624**, 1097
 Bennett, C. J., Osamura, Y., Lebar, M. D., & Kaiser, R. I. 2005b, *ApJ*, **634**, 698
 Bergantini, A., Góbi, S., Abplanalp, M. J., & Kaiser, R. I. 2018, *ApJ*, **852**, 70
 Bergantini, A., Maksyutenko, P., & Kaiser, R. I. 2017, *ApJ*, **841**, 96
 Bernstein, M. P., Sandford, S. A., Allamandola, L. J., et al. 1999, *Sci*, **283**, 1135
 Boamah, M. D., Sullivan, K. K., Shulenberger, K. E., et al. 2014, *FaDi*, **168**, 249
 Bossa, J.-B., Ordu, M. H., Müller, H. S. P., Lewen, F., & Schlemmer, S. 2014, *A&A*, **570**, A12
 Bouilloud, M., Fray, N., Bénilan, Y., et al. 2015, *MNRAS*, **451**, 2145
 Braakman, R., Drouin, B. J., Widicus Weaver, S. L., & Blake, G. A. 2010, *JMoSp*, **264**, 43
 Briggs, R., Ertem, G., Ferris, J. P., et al. 1992, *OLEB*, **22**, 287
 Brown, R. D., Crofts, J. G., Godfrey, P. D., et al. 1975, *ApJ*, **197**, L29
 Butscher, T., Duvernay, F., Danger, G., & Chiavassa, T. 2016, *A&A*, **593**, A60
 Cazaux, S., Tielens, A. G. G. M., Ceccarelli, C., et al. 2003, *ApJ*, **593**, L51
 Cooper, G., Reed, C., Nguyen, D., Carter, M., & Wang, Y. 2011, *PNAS*, **108**, 14015
 de Marcellus, P., Meinert, C., Nuevo, M., et al. 2011, *ApJL*, **727**, L27
 Dibenedetto, A., Aresta, M., Giannoccaro, P., et al. 2006, *Eur. J. Inorg. Chem.*, **2006**, 908
 Drouin, D., Couture, A. R., Joly, D., et al. 2007, *Scanning*, **29**, 92
 Eckhardt, A. K., Bergantini, A., Singh, S. K., Schreiner, P. R., & Kaiser, R. I. 2019, *AngCh*, **58**, 5663
 Fedoseev, G., Chuang, K. J., Ioppolo, S., et al. 2017, *ApJ*, **842**, 52
 Frisch, M. J., Trucks, G. W., Schlegel, H. B., et al. 2009, *Gaussian 09*, Revision D.01 (Gaussian Inc.: Wallingford, CT)
 Fuente, A., Cernicharo, J., Caselli, P., et al. 2014, *A&A*, **568**, A65
 Garrod, R., Hee Park, I., Caselli, P., & Herbst, E. 2006, *FaDi*, **133**, 51
 Garrod, R. T., Weaver, S. L. W., & Herbst, E. 2008, *ApJ*, **682**, 283
 Gibb, E. L., Whittet, D. C. B., Boogert, A. C. A., & Tielens, A. G. G. M. 2004, *ApJS*, **151**, 35
 Góbi, S., Crandall, P. B., Maksyutenko, P., Förstel, M., & Kaiser, R. I. 2018, *JPCA*, **122**, 2329
 Herbst, E. 2021, *FrASS*, **8**, 207
 Herbst, E., & van Dishoeck, E. F. 2009, *ARA&A*, **47**, 427
 Hollis, J. M., Lovas, F. J., & Jewell, P. R. 2000, *ApJ*, **540**, L107
 Holtom, P. D., Bennett, C. J., Osamura, Y., Mason, N. J., & Kaiser, R. I. 2005, *ApJ*, **626**, 940
 Hudson, R. L., Loeffler, M. J., Ferrante, R. F., Gerakines, P. A., & Coleman, F. M. 2020, *ApJ*, **891**, 22
 Jones, B. M., & Kaiser, R. I. 2013, *JPCL*, **4**, 1965
 Jørgensen, J. K., Favre, C., Bisschop, S. E., et al. 2012, *ApJL*, **757**, L4
 Kaiser, R. I. 2002, *ChRv*, **102**, 1309
 Kaiser, R. I., Eich, G., Gabrysch, A., & Roessler, K. 1997, *ApJ*, **484**, 487
 Kaiser, R. I., Maity, S., & Jones, B. M. 2014, *PCCP*, **16**, 3399
 Kaiser, R. I., Maity, S., & Jones, B. M. 2015, *Angew. Chem., Int. Ed.*, **54**, 195
 Kaiser, R. I., Stockton, A. M., Kim, Y. S., Jensen, E. C., & Mathies, R. A. 2013, *ApJ*, **765**, 111
 Kisiel, Z., Pszczółkowski, L., Białkowska-Jaworska, E., & Charnley, S. B. 2016, *JMoSp*, **321**, 13
 Kitadaï, N., & Maruyama, S. 2018, *GeoFr*, **9**, 1117
 Kleimeier, N. F., Eckhardt, A. K., & Kaiser, R. I. 2021, *JACS*, **143**, 14009
 Kleimeier, N. F., Eckhardt, A. K., Schreiner, P. R., & Kaiser, R. I. 2020, *Chem*, **6**, 3385
 Kleimeier, N. F., & Kaiser, R. I. 2021, *ChemPhysChem*, **22**, 1229
 Kleimeier, N. F., & Kaiser, R. I. 2022, *JPCL*, **24**, 229
 Köck, E.-M., Bernard, J., Podewitz, M., et al. 2020, *CEJ*, **26**, 285
 Kostko, O., Bandyopadhyay, B., & Ahmed, M. 2016, *ARPC*, **67**, 19
 Linden, M. M., Wagner, J. P., Bernhardt, B., et al. 2018, *JPCL*, **9**, 1663
 Maity, S., Kaiser, R. I., & Jones, B. M. 2014, *FaDi*, **168**, 485
 McMurtry, B. M., Saito, S. E. J., Turner, A. M., Chakravarty, H. K., & Kaiser, R. I. 2016, *ApJ*, **831**, 174
 Meinert, C., Myrgorodska, I., de Marcellus, P., et al. 2016, *Sci*, **352**, 208
 Milligan, D. E., & Jacox, M. E. 1971, *JChPh*, **54**, 927
 Montgomery, J. A., Frisch, M. J., Ochterski, J. W., & Petersson, G. A. 1999, *JChPh*, **110**, 2822
 Montgomery, J. A., Frisch, M. J., Ochterski, J. W., & Petersson, G. A. 2000, *JChPh*, **112**, 6532
 Morton, R. J., & Kaiser, R. I. 2003, *P&SS*, **51**, 365
 Muñoz Caro, G. M., Meierhenrich, U. J., Schutte, W. A., et al. 2002, *Natur*, **416**, 403
 Neill, J. L., Muckle, M. T., Zaleski, D. P., et al. 2012, *ApJ*, **755**, 153
 Nuevo, M., Auger, G., Blanot, D., & D'Hendecourt, L. 2008, *OLEB*, **38**, 37
 Nuevo, M., Bredehöft, J. H., Meierhenrich, U. J., d'Hendecourt, L., & Thiemann, W. H.-P. 2010, *AsBio*, **10**, 245
 Nuevo, M., Chen, Y. J., Yih, T. S., et al. 2007, *AdSpR*, **40**, 1628
 Paardekooper, D. M., Fedoseev, G., Riedo, A., & Linnartz, H. 2016, *A&A*, **596**, A72
 Parise, B., Ceccarelli, C., Tielens, A. G. G. M., et al. 2002, *A&A*, **393**, L49
 Peltzer, E. T., & Bada, J. L. 1978, *Natur*, **272**, 443
 Peltzer, E. T., Bada, J. L., Schlesinger, G., & Miller, S. L. 1984, *AdSpR*, **4**, 69
 Petrie, S. 1995, *ApJL*, **454**, L165
 Plankensteiner, K., Reiner, H., & Rode, B. 2005, *Curr. Org. Chem.*, **9**, 1107
 Reisenauer, H. P., Wagner, J. P., & Schreiner, P. R. 2014, *Angew. Chem., Int. Ed.*, **53**, 11766
 Rivilla, V. M., Colzi, L., Jiménez-Serra, I., et al. 2022, *ApJL*, **929**, L11
 Ruscic, B., & Bross, D. H. 2021, Active Thermochemical Tables (ATcT) values based on ver. 1.122r of the Thermochemical Network, <https://atct.anl.gov/Thermochemical%20Data/version%201.122r/index.php>
 Socrates, G. 2004, *Infrared and Raman Characteristic Group Frequencies: Tables and Charts* (Chichester: Wiley)
 Song, X., Li, J., Hou, H., & Wang, B. 2006, *JChPh*, **125**, 094301
 South, P. F., Walker, B. J., Cavanagh, A. P., et al. 2017, *Plant Cell*, **29**, 808
 Turner, A. M., Abplanalp, M. J., Chen, S. Y., et al. 2015, *PCCP*, **17**, 27281
 Turner, A. M., Bergantini, A., Koutsogiannis, A. S., et al. 2021, *ApJ*, **916**, 74
 Turner, A. M., & Kaiser, R. I. 2020, *AcChR*, **53**, 2791
 van Scheltinga, J. T., Marcandalli, G., McClure, M. K., Hogerheijde, M. R., & Linnartz, H. 2021, *A&A*, **651**, A95
 White, G. J., Araki, M., Greaves, J. S., Ohishi, M., & Higginbottom, N. S. 2003, *A&A*, **407**, 589
 Yeghikyan, A. G. 2011, *Ap*, **54**, 87
 Zheng, W., Jewitt, D., & Kaiser, R. I. 2007, *CPL*, **435**, 289
 Zhou, Y., Quan, D.-H., Zhang, X., & Qin, S.-L. 2020, *RAA*, **20**, 125
 Zhu, C., Bergantini, A., Singh, S. K., et al. 2021, *ChCom*, **57**, 4958
 Zhu, C., Frigge, R., Bergantini, A., Fortenberry, R. C., & Kaiser, R. I. 2019, *ApJ*, **881**, 156
 Zhu, C., Kleimeier, N. F., Turner, Andrew, M., et al. 2022, *PNAS*, **119**, e2111938119
 Zhu, C., Turner, A. M., Abplanalp, M. J., et al. 2020a, *ApJL*, **899**, L3
 Zhu, C., Turner, A. M., Meinert, C., et al. 2020b, *ApJ*, **889**, 134